Scientific Research Publishing

Open Journal of Geology, 2024, 14, 823-854
https://www.scirp.org/journal/ojg
ISSN Online: 2161-7589
ISSN Print: 2161-7570

Application of Remote Sensing and GIS in Mineral Alteration Mapping and Lineament Extraction Case of Oudiane Elkharoub (Requibat Shield, Northern of Mauritania)

Ould Mahmoud Hdeid[1], Yousra Morsli[1], Mohamed Raji[1], Zouhir Baroudi[1], Malika Adjour[1], Khaled Cheikh Nebagha[2], Zein El Arby[2], Vetah Mohamed El Moktar[3], Isselmou Brahim Vall[3]

[1]Department of Geology, Faculty of Sciences Ben M'sik, Hassan II University, Casablanca, Morocco
[2]Department of Geology, Faculty of Sciences and Technology, University of Nouakchott Al Asriya, Nouakchott, Mauritania
[3]National Agency for Geological Research and Mining Heritage, Nouakchott, Mauritania
Email: Hdeid.mahmoud2071@gmail.com

How to cite this paper: Hdeid, O.M., Morsli, Y., Raji, M., Baroudi, Z., Adjour, M., Nebagha, K.C., El Arby, Z., El Moktar, V.M. and Vall, I.B. (2024) Application of Remote Sensing and GIS in Mineral Alteration Mapping and Lineament Extraction Case of Oudiane Elkharoub (Requibat Shield, Northern of Mauritania). *Open Journal of Geology*, **14**, 823-854.
https://doi.org/10.4236/ojg.2024.149036

Received: April 22, 2024
Accepted: September 9, 2024
Published: September 12, 2024

Abstract

The integration of remotely sensed data allowed the successful characterization of the mineral alteration zones of the Oudiane Elkharoub area in the Northeastern part of Reguibat Shield using image transformation techniques. As both chemical and geochemical analyses showed significant Au, Ag, Cu, Pb, Mn, Cr, Ni, Th and Y anomalies, it's very interesting to apply the remote sensing and GIS in mineral resources mapping. The remote sensing is a direct adjunct to the field, lithologic and structural mapping, and more recently, GIS has played an important role in the study of mineralization areas. The integration of several evidential maps highlighted the plausible areas with high concentrations of chlorite, epidote, kaolinite, calcite, alunite, hematite, illite and sulfur among other key mineral alterations that reflect the intensity of hydrothermal effects and the probable sites of ore bodies. The methodological approach integrates geological information acquired from Aster and Landsat 8 OLI/TIRS (Operational Land Imager/Thermal InfraRed Sensor) images and a multi-criteria GIS analysis. The superimposition of various lineament and hydrothermal alteration maps and the consideration of precious and base metal indicators allowed the zoning of sites likely to contain mineral concentrations. Remote sensing becomes an important tool for locating mineral deposits in its own right, when the primary and secondary processes of mineralization result in the formation of spectral anomalies. Reconnaissance lithological mapping is usually the first step of mineral resource mapping. This is complimented with structural mapping, as mineral deposits usually occur along or adjacent

to geologic structures, and alteration mapping, as mineral deposits are commonly associated with hydrothermal alteration of the surrounding rocks. Ground truthing and laboratory studies including XRD analysis were utilized to verify the results.

Keywords

Remote Sensing, GIS, ASTER, Landsat 8 (OLI/TIRS), Structure, Mineralization, Alteration, Mineral, Lineament, Reguibat Shield, Oudiane Elkharoub

1. Introduction

Satellite remote sensing provides valuable spatial and temporal information on the Earth's resources. Since NASA's first Landsat satellite was launched in 1972, key advances have been made in the field of geological reconnaissance including mining exploration [1]. Mineral resources originating from hydrothermal activity have been identified using remotely sensed data. The variable spatial, radiometric and spectral resolution of modern remote sensing data presents opportunities for targeting potential areas for new mineral prospects [1] [2]. Hydrothermal activity occurring through fracture/fault zones modifies the physical and chemical properties of the country rock [3]. The characterization of hydrothermal alteration zones and their grade is important for identifying potential areas of mineral resources [1] [4] [5], as the metals have a tendency to occur in the most highly altered rocks [3]. Several studies have been performed using optical Near Infrared (NIR) and Shortwave Infrared (SWIR) remote sensing data to identify hydrothermal alteration zones [2] [6]-[10]. Landsat data have long been successfully employed for locating hydrothermal alteration zones [6] [8] [11] [12]. However, the launch of the Advanced Space Borne Thermal Emission and Reflection Radiometer (ASTER) satellite in 1999 allowed the identification of key hydrothermal minerals [10] [13]-[17]. Compared to other multispectral data, the spectral, spatial and radiometric resolution of ASTER data is superior [15] [18] [19]. In the last two decades, ASTER data have been successfully used to identify hydrothermal alteration zones for mineral resources prospecting [10] [14] [16] [20]-[23]. ASTER was the first multispectral space-borne sensor capable of identifying OH-bearing minerals using its 14 spectral bands, particularly those minerals within the SWIR region [2] [14] [18]. The characterization of key hydrothermally altered mineral assemblages and the definition of the geometry of the hydrothermal alteration zones using ASTER data was found to be effective for identifying potential areas of mineral resources [14] [24] [25]. SWIR data has allowed the identification of specific categories of hydrothermal minerals, such as phyllosilicates, clays, carbonates, and sulfates, depending on their spectral signatures [2]. Several approaches, such as Principal Component Analysis (PCA), the use of band ratios, Relative Absorption Band Depth (RBD) [26] and mineral indices [2] [9] [22], and spectral analysis have been employed to analyze multispectral data. Band ratios

have been used to analyze the spectral characteristics between bands and minimize topographic influences [7] [8] [27]-[29]. Hydrothermally altered mineral assemblages can be categorized based on the intensity of the hydrothermal activity [14] [24] [25] [27] [30]. Sub-pixel spectral classifications can therefore be assigned to specific key hydrothermal minerals that relate to propylitic (epidote, chlorite, calcite), phyllic (muscovite, sericite, illite), argillic (montmorillonite, kaolinite, dickite), and advanced argillic (alunite-pyrophyllite) zones of alteration. Geographic Information System (GIS) tools have been used to produce integrative maps through digital overlay methods [14] [31] [32]. Knowledge-driven approaches integrating multi-criteria decision-making depending on expert judgement have also been used to produce predictive maps [33] [34]. Such approaches employ ranked binary evidential maps. Several evidential maps can therefore be combined to obtain prospective maps [35]. In this study, we tested the application of these data and remote sensing approaches for the identification of hydrothermal alteration zones and lineaments extraction in the study area of the Oudiane Elkaroub, Reguibat shield, Birimian domain, which is characterized by a dry environmental setting and a lack of vegetation. The analysis of ASTER and Landsat 8 is necessary to enable the future mapping of the spatial distribution of mineral alteration zones, indicating the nature of the mineral resources' prospects in the area, as well as the identification of the lineament's extraction.

Mineral resources mapping is an important type of geologic mapping activity and usually covers a great part of varied studies, focused on spectral analysis, structural mapping, identification of hydrothermal alteration zone [36], mineral alteration mapping [37], ferric oxide and oxhydroxide mineral mapping [38], gold exploration [39], hyperspectral imagery [40], integration with Geographic Information System (GIS) [41], etc. Because most of the surface and near-surface mineral deposits in accessible regions of the Earth have been found, current emphasis is on the location of deposits far below the Earth's surface or in inaccessible regions. Geophysical methods that provide deep penetration into the Earth are generally needed to locate potential deposits and drill holes are required to confirm their existence.

However, much information about potential areas for mineral exploration can be provided by interpretation of surface features on aerial photographs and satellite images.

2. Regional Geological Context

The West African Craton is subdivided into three distinct domains (**Figure 1**), [42]-[45]. 1) In the north, the Reguibat Shield outcropping in Mauritania, Algeria, and Morocco, constituted by Archean formations (3.0 - 2.7 Ga) and Paleoproterozoic (~2 Ga). 2) In the south, the Man or Leo Shield was formed by the Archean series of the Liberian Shield and the Paleoproterozoic formation of the Baoule-Mossi Domain covering Ghana, Ivory Coast, Guinea, southern Mali, Burkina Faso, western Niger; these Paleoproterozoic formations are generally referred to

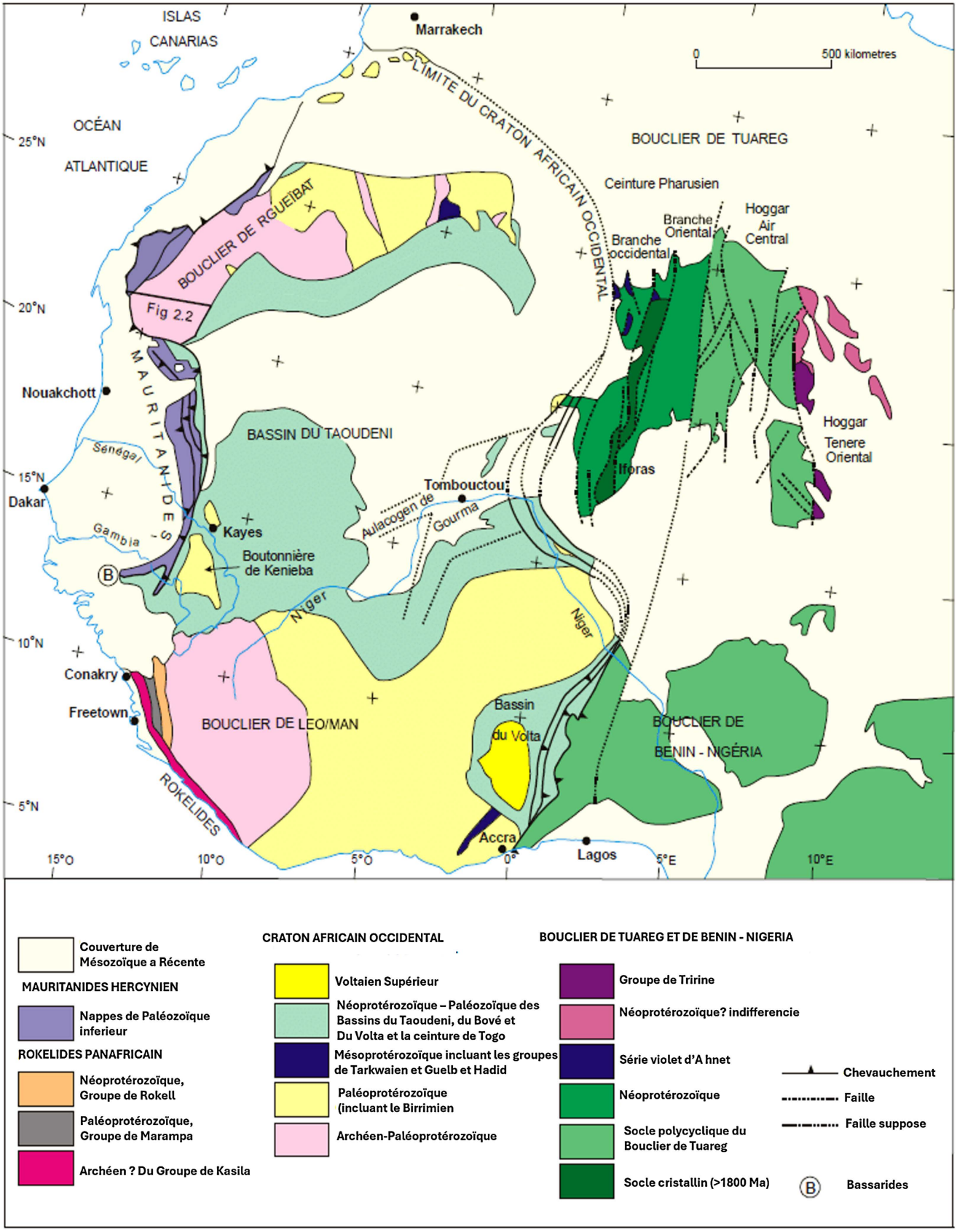

Figure 1. Geology of the West African Craton. Modified from [46].

as Birimian. 3) In an intermediate position between the two dorsal, two buttonholes, the Kayes buttonholes in western Mali and the Kedougou Buttnhole located on either side of the border Senegales-Malian; these buttonholes are formed exclusively by Birimian series.

There are five principal geological entities within the borders of Mauritania (**Figure 2**). One of these, the Reguibat Shield, is located to the north of the country. It hosts Archean and Paleoproterozoic metamorphic sequences and granites that form the northwestern limit of the West African Craton (WAC) [47] [48]. Further to the south, the Craton's margins coincide with the Mauritanide Belt (**Figure 2**), a Hercynian tectonic belt consisting of Neoproterozoic and Paleozoic metamorphosed sediments and volcanoclastic formations, including parts of the underlying basement [49]. To the east of the Mauritanide Belt lies the vast Mesoproterozoic [50] to-Paleozoic Taoudeni Basin. Finally, to the west lies the northern limit of Mauritania-Senegal-Gambia-Conakry basin, a Mesozoic-Cenozoic continental margin-type basin that overlies a Paleozoic (and probably Archean) basement. Mauritania is a significant source for gold, iron and copper ores in African continent. It was the second-highest-ranked exporter and producer of iron in Africa in 2012, being preceded only by South Africa. In addition to iron, Mauritania also produces cement, copper, crude oil, gas, gold, gypsum, quartz, salt and steel [51]. The Birimian terrains (2156 ± 10 to 2067 ± 12 Ma) of the West Africa Craton are one of enormous interest, both for their fundamental potential in terms of geological research and in terms of mining. Indeed, they are some of the oldest lands in the Craton, and are affected by important orogenies. The Birimian rocks host many gold deposits and occurrences of the West Africa Craton. They were formed and accreted during the Eburnean orogenic cycle, which took place between 2.25 Ga and 1.80 Ga. The Birimian hosts some of the main types of such deposits in West Africa Craton, and these are directly associated with granitic plutons. This type of environment is, in turn, the supplier of relevant metals such as Au, Ag, Pb and Zn, which are associated with many types of deposits (copper porphyries, perigranitic veins, skarns, etc.). As such, they are major economic targets. In addition, perigranitic deposits contain gold, which has become the subject of abundant and extensive geological discussion, leading to varied and novel terminologies. The Mauritanian Birimian terrains are, however, yet to be properly known.

The study zone is located in the Gallaman in the central part of Reguibat Shield (**Figure 2**), which has been stable since about 1700 Ma [42] and dominates the north third of Mauritania's geological surface. This choice is based on the fact that despite the scare amount of research on the study zone, as a part of Reguibat Shield, the Oudiane Elkharoub Zone has the same characteristics as the lager area it constitutes, possessing many precious and base metals. The objective is to figure out the anomalies for precious and base metals and define the type of mineralization (Auriferous, Polymetallic, etc.). This work contributes on the one side to a better understanding and planning of subsequent research activities and exploration, on the side to improvement of geological knowledge on Oudiane Elkharoub

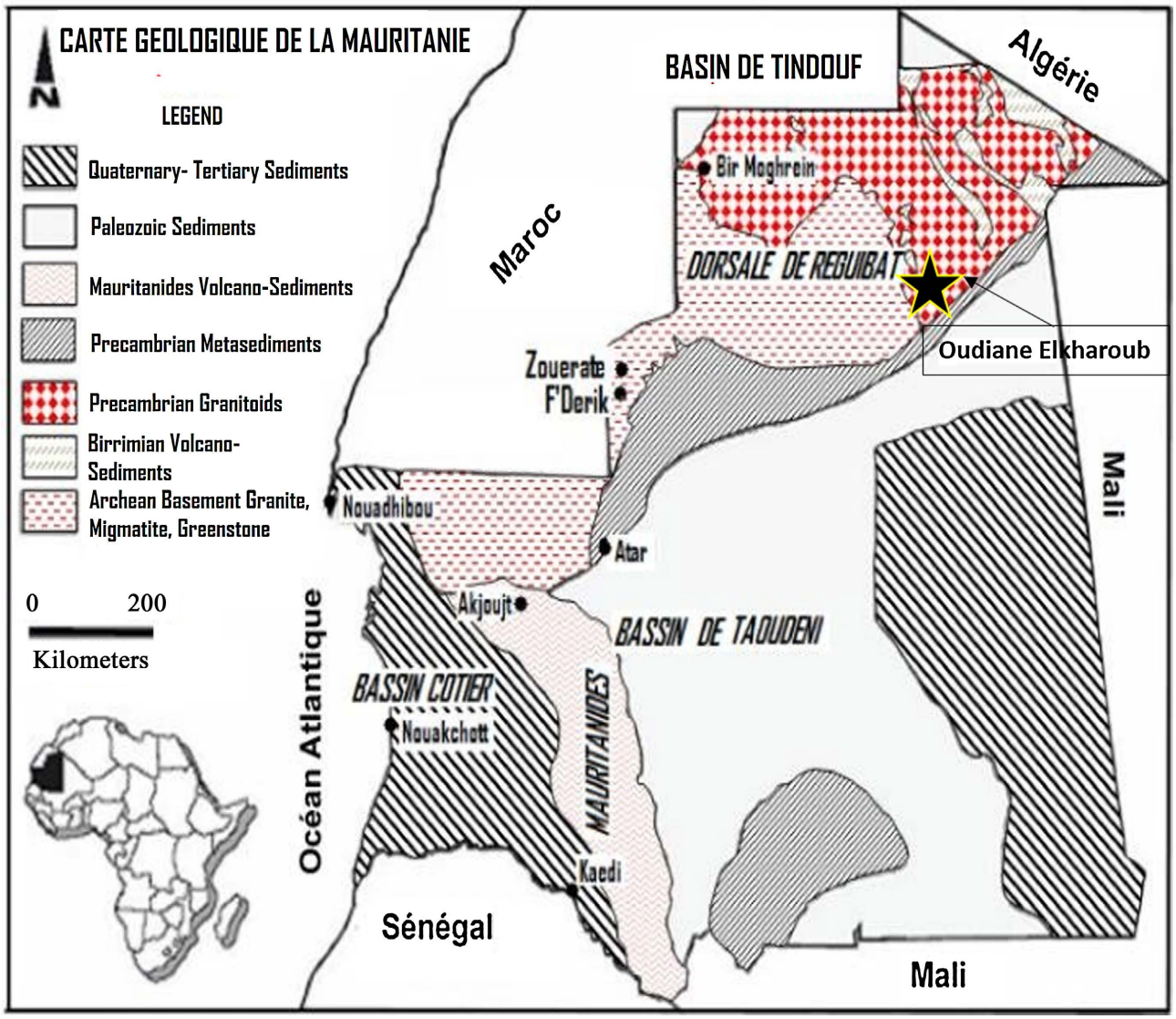

Figure 2. Simplified geological map of Mauritania.

Zone, which presents all the specificity to host all type of mineralization.

3. Geological Overview of the Oudiane Elkharoub Zone

As mentioned above, the Oudiane Elkharoub Zone is in the so-called Ghallaman Group, in the central part of the Reguibat Shield (**Figure 3**). Rocci [42] has described the occurrences of leptynite, pyroxene gneisses (a diopside gneiss and diospide + hyperstene gneiss) and amphibolite, as well as much rarer outcrops of cipolins and two-mica gneisses.

According to [42] [52]-[54], the Temmimichate Group differs from the Ghallaman Group given the omnipresence of granulitic gneiss. The author indicates that the sebkhat of Ghallaman Group correspond to all outcrop of metamorphic rocks located to the east of large sebkhas of the same name within it. Rocci note the presence of the following: two meca gneisses, amphibolite, pyroxene

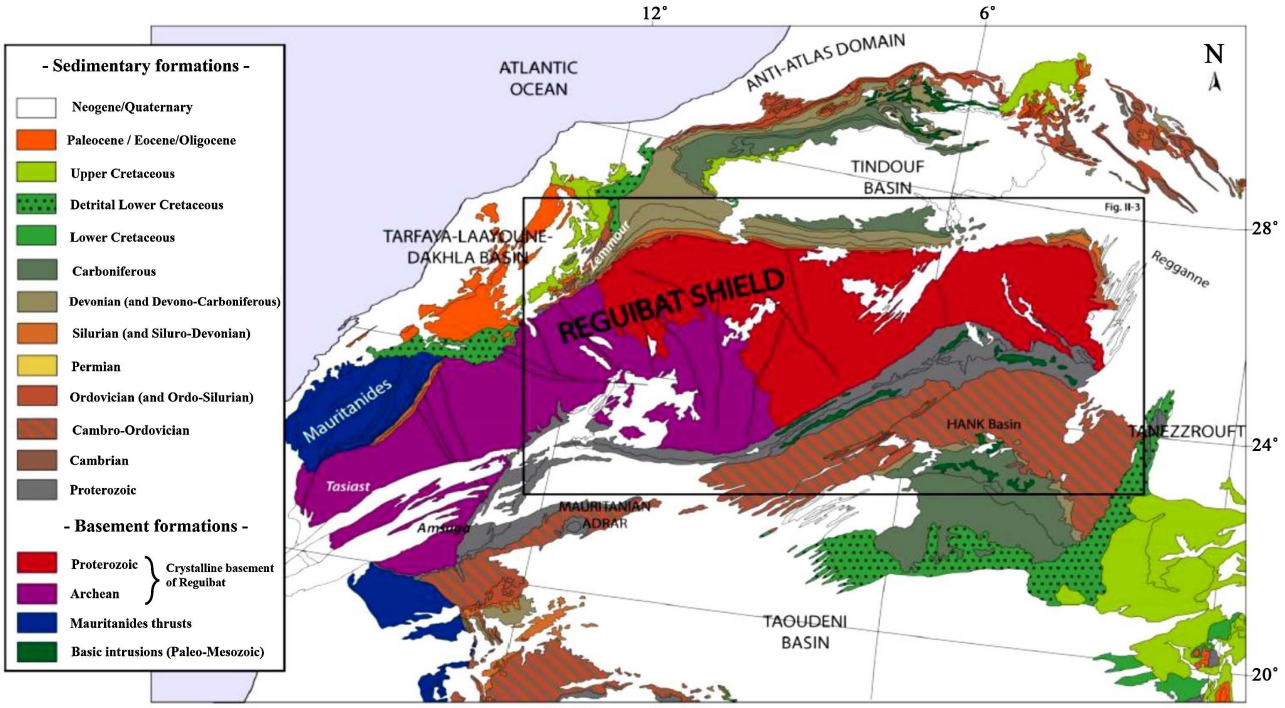

Figure 3. Geological map presenting the West African Craton, centered on the Reguibat shield [57].

gneiss and leptynite. The group of sebkhas at the Oudiane Elkharoub Zone emerge in serie of sumeridian depressions that converge in their descension from the Alous Tmar hills. For [42] [55], they differ very clearly from the previous sabkhas due to the great homogeneity of the facies that compose them, as well as to the existence of aluminous-to-hyperaluminous gneisses. The observation on field mapping coupled with the local geophysical map show a geological and structural complexity in the study zone (**Figure 4**) that reinforces its significance to be an interesting zone to hosting the mineralization. Moreover, its location is particularly special, seen, as it is set between two batholiths with different age: to the west, it is the tmemeimichat Ghallaman granitoid (dated 2150-2100 Ma) and to the east the Yetti granitoids (dated 2050-1995 Ma) [56]. All these geological and structural complexity make a good argument for the discovery of large deposits in Oudiane Elkharoub zone.

4. Material and Methods

4.1. Mineral Alteration

The Oudiane Elkharoub Zone (location coordinate: 542250, 2611070) is located within the central eastern part of Reguibat Shield, in the administrative region (Willaya) of Tiriss Zemmour 450 km to the northeast of an Iron deposit (Kediat Ijil, exploiting by National Industrial and Mining Company (SNIM) in the city of Zeouarat, northern Mauritania.

ASTER data was collected on-board the TERRA spacecraft in May 2007 by NASA. The spectral channels of ASTER were acquired from the NASA Land

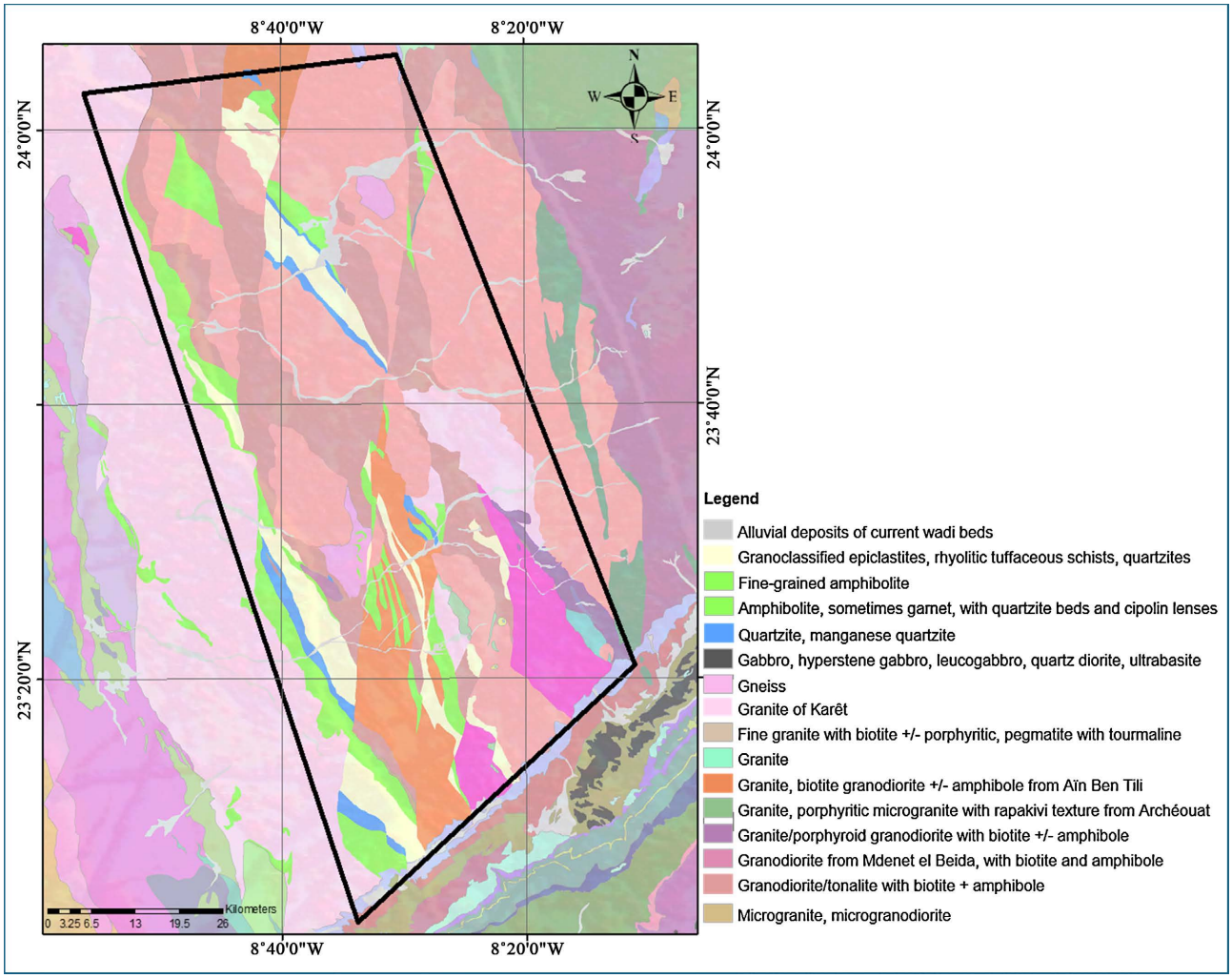

Figure 4. Geological and structural map of Oudine Elkharoub after [53]-[56].

Processes Distributed Active Archive Center (LP DAAC). Three categories of spectral information were collected, including three VNIR bands, six SWIR bands and four TIR bands. The SWIR bands were transformed into valuable information using ENVI v.5.4. The ASTER SWIR spectral bands that recorded electromagnetic radiation between the wavelengths of ~1.60 and 2.45 μm were used to discriminate between the absorption signatures of different groups of hydrothermal minerals, including Fe/Mg-OH, Al-OH, and CO_3 [19]. One scene from the ASTER cloud-free level (in HDF file format, 1B bands acquired on 7 October 2007) was analyzed in the area of interest. This level of processed radiance recorded at the sensor (in $Wm^{-2}{\cdot}sr^{-1}{\cdot}\mu m^{-1}$) is derived from level 1A by correcting the geometric distortion and applying the radiometric coefficient. The pre-processing step included cross-talk improvements and orthorectification of bands. The data was georegistered to zone 29 of the Universal Transverse Mercator (UTM) World Geodetic System 1984 (WGS84) using ENVI software. In order to standardize and minimize the disturbances due to the atmosphere, altitude, sensors and sun radiance, a log-residual algorithm was applied to the SWIR bands [16] [58]. Spectral angle mapping was

implemented on the normalized data using spectra extracted from the imagery and the spectra of alteration minerals selected from the United States Geological Survey (USGS) spectral library and NASA's Jet Propulsion Laboratory (JPL) and resampled to ASTER spectral resolution (Figure 5).

The Spectral Angle Mapper (SAM) is one of the available techniques for mapping of hydrothermal alteration minerals. It is a classification method for comparing image spectra to individual spectra or a spectral library [59]. This technique calculates the angular distance between each spectrum in the image and the reference spectra or endmembers in n-dimensions (Figure 6). This result is a classification image showing the best SAM match at each pixel and a Rule image for each endmember showing the actual angular distance in radians between each spectrum in the image and the reference spectrum. Darker pixels in the rule images represent smaller spectral angles, and thus spectra that are more similar to

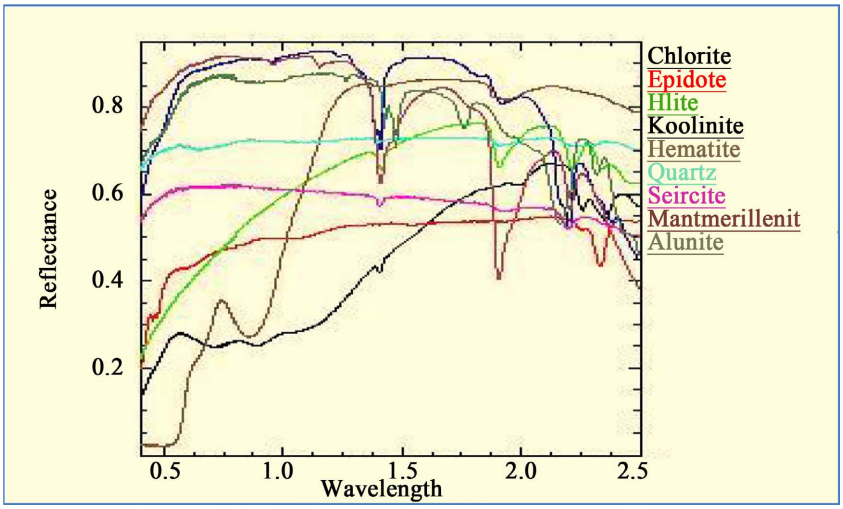

Figure 5. The USGS library spectra of the studied minerals superimposed on ASTER data band intervals in the VNIR-SWIR region.

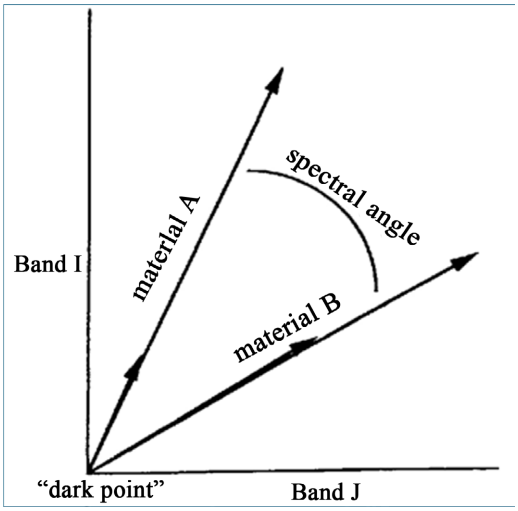

Figure 6. Two-dimensional example of the Spectral Angle Mapper.

the reference spectrum. The rule images can be used for subsequent classification using different thresholds to decide which pixels are included in the SAM classification image (ENVI User's Guide, 2003).

The Minimum Noise Fraction (MNF) transformation [60] was applied to obtain a pixel purity index in order to extract the highest number of spectrally pure pixels from the input MNF data. These results were used to define end-members using multidimensional visualization for spectral classification, to guide the mineral characterization. In order to validate the results, we used as references the field mapping, the samples from the field and the most update maps covering the study area. The use of Aster data in mineral prospecting has increased in recent years because its relatively low cost, broad coverage, and unique integral bands highly sensitive to mineral alteration (minerals known to surround target minerals) (**Figure 7**) illustrates two classical alteration models showing hydrothermal alteration zones associated with some copper and gold deposits.

For example, Kaolinite is common alteration product associated with both gold and copper deposits. Hence, mapping concentrations of kaolinite using ASTER can indicate the presence of these ore. The ASTER data set contain visible, shortwave infrared and thermal bands. The proper preprocessing and combination of these bands can produce relative mineral alteration distribution such as iron oxides, siliceous rocks, carbonates, sericite, illite, alunite and kaolinite. Because some of spectral bands of ASTER are found to be sensitive to some of these above-mentioned clays and iron absorptions, Borstad Associates Ltd. offers a suite of standards ASTER alteration enhancement that can be used to broadly delineate these mineral zones or assemblages.

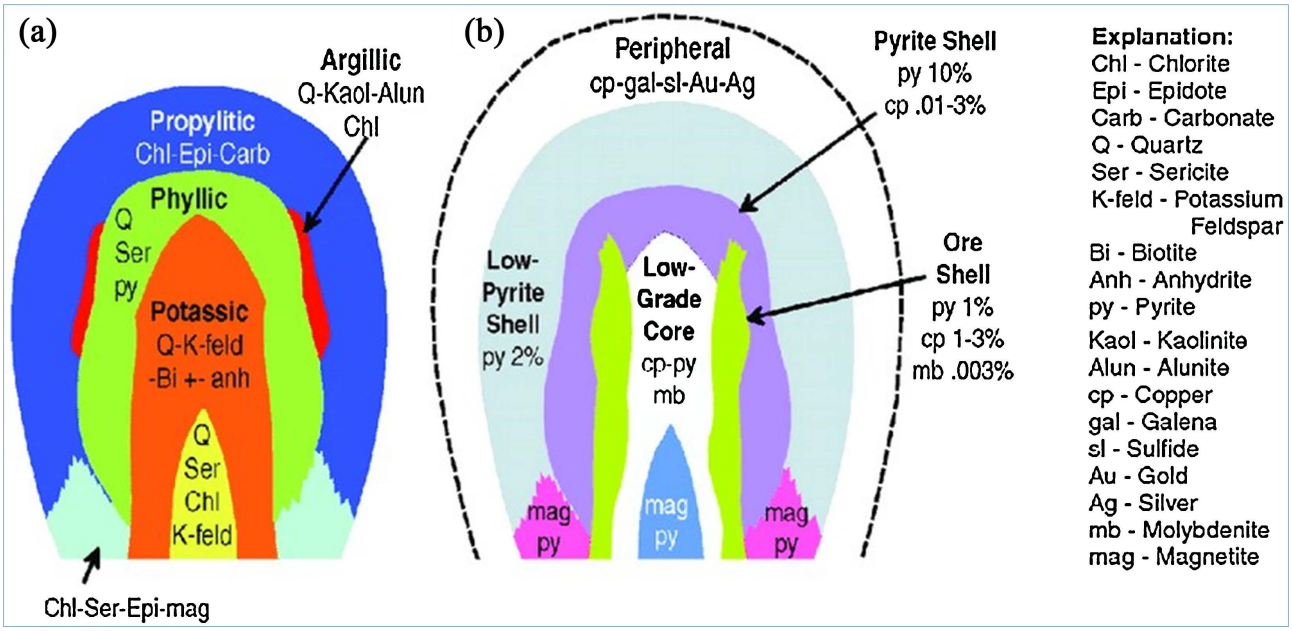

Figure 7. Hydrothermal alteration zones associated with porphyry copper deposit (modified after [61]. (a) Schematic cross section of hydrothermal alteration mineral zones, which consist of propylitic, phyllic, argillic and potassic alteration zones. (b) Schematic cross section of ores associated with each alteration zone.

The ASTER level-1T is radiometrically calibrated and was pre-georeferenced to a UTM zone 29 north Projection using the WGS-84 datum. A "crosstalk" instrument problem happened due to leakage of photons from one detector to another spastically from band 4 to bands 5 and 9, which are affected by offset in radiance in the ASTER SWIR data by detector leakage the crosstalk correction can be used for AST_LIT data [62]. This correction is applied to SWIR data to remove the effect of energy overspill from b4 to b5 and b9. The VNIR and SWIR datasets were resampled by using the cubic convolution technique and stacked into a file. Therefore, the nine bands have the same 15 × 15 pixel as VNIR. The SWIR bands were stacked with VNIR images to produce nine band ASTER images with 15 m size (VNIR + SWIR). For resampling, the nearest neighbour resampling method is used to preserve the original values. The Fast of Sight Atmospheric Analysis of the Spectral Hypercubus (FLAASH) was used for atmospheric correction on the 9 bands of ASTER [63]. This algorithm has the standard MODTRAN model atmospheres [64]. We describe parameters used in FLAASH for one scene used. The atmospheric correction is applied based on solar zenith angle, satellite view angle, and the relative angle between the satellite and sun image parameters.

Overall, ten ASTER level IT precision terrain registered at sensor radiance (AST_LIT) scenes cover the study area and were used for mapping alteration mineral zones. The dataset is in Hierarchical Data Format (HDF). The data used in this study were collected from the USGS Earth Explorer Website at https://earthexplorer.usgs.gov/. The satellite remote sensing dataset was processed by ENVI (Environment for Visualizing Images) version 5.3, QGIS and Arc GIS version 10.8 software. ASTER has 14 spectral bands with 60 km swath width (each scene represents a 60 × 60 km^2 area) [65]. The first three bands are visible and near-infrared (VNIR1/4 0.52 to 0.86 mm) with a 15 m spatial resolution. The next six bands are in the shortwave infrared (SWIR1/4 1.6 to 2.43 mm) with 30m spatial resolution, and the last five bands are thermal infrared (TIR1/4 8.13 to 11.65 mm) with 90 m spatial resolution [65]. The VNIR infrared bands highlight iron oxide [26] and the SWIR bands can be applied to detect hydrothermal alteration assemblages [20]. In this study, ASTER NVIR + SWIR is used. The methodology of this research is summarized with a simple flowchart (**Figure 8**).

4.2. Lineament Extraction

The image used is Landsat 8 OLI/TIRS (Path 201 and Row 43 and 44 taken on 10 May 2023) and the data is available free at the United States Geological Survey website (https://earthexplorer.usgs.gov/). It is provided with the Universal Transverse Mercator (UTM) projection and a WGS 84 World Geodetic System. This image contains eleven bands with different wavelengths and resolutions (**Table 1**) from Landsat 8 image. The most used band in geology are the optical bands (OLI) from the Coastal aerosol to the panchromatic band. The main step of lineament extraction is described in the following chart (**Figure 9**). It starts with pre-processing, consisting of radiometric and atmospheric corrections, then the

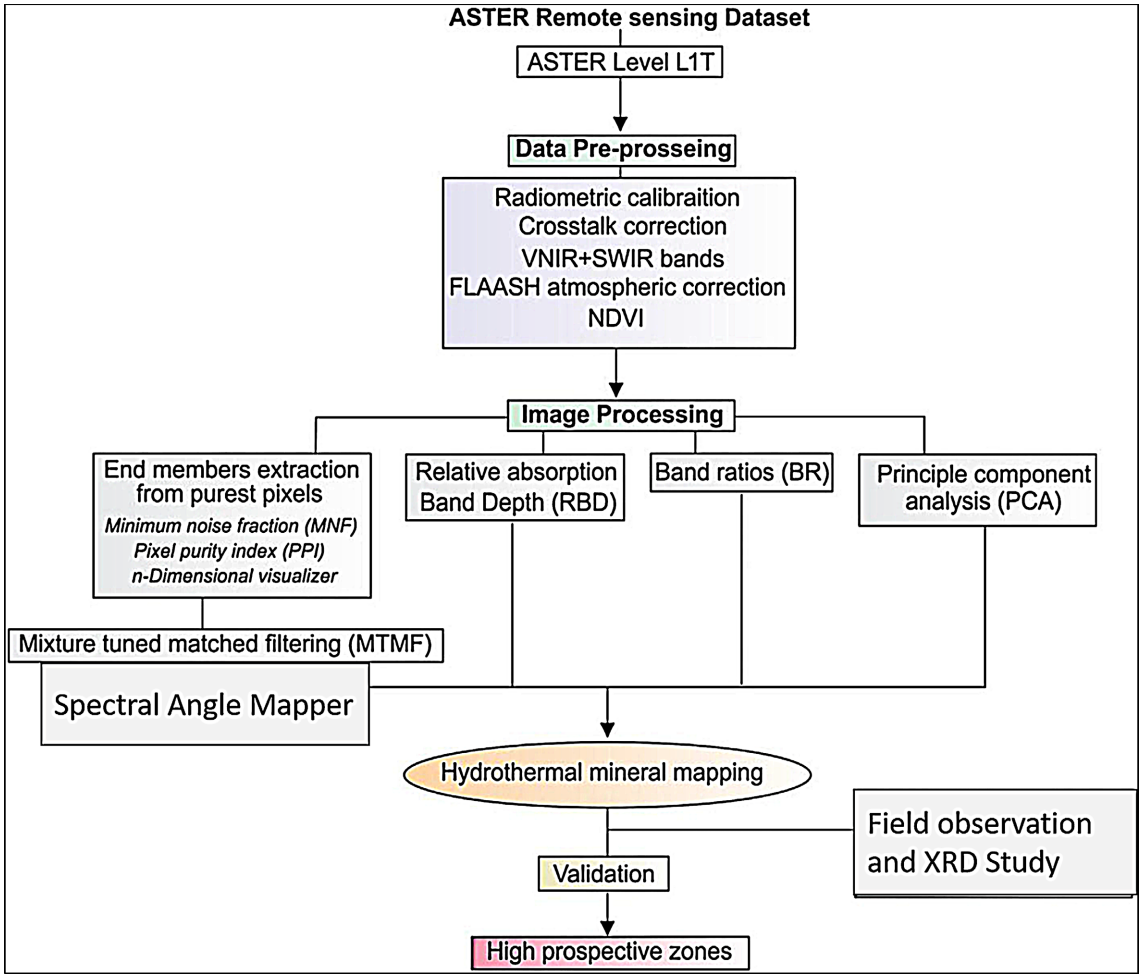

Figure 8. Simplify methodology flowchart in this research for mineral alteration.

Table 1. Spectral bands of the Landsat 8 satellite [70] [71].

Bands		Wavelengths (μm)	Spatial resolution (m)
Band 1	Coastal aerosol	0.43 - 0.45	30
Band 2	Blue	0.45 - 0.51	30
Band 3	Green	0.53 - 0.59	30
Band 4	Red	0.64 - 0.67	30
Band 5	NIR	0.85 - 0.88	30
Band 6	SWIR1	1.57 - 1.65	30
Band 7	SWIR2	2.11 - 2.29	30
Band 8	Panchromatic	0.50 - 0.68	15
Band 9	Cirrus	1.36 - 1.38	30
Band 10	TIRS1	10.60 - 11.19	100
Band 11	TIRS2	11.50 - 12.51	100

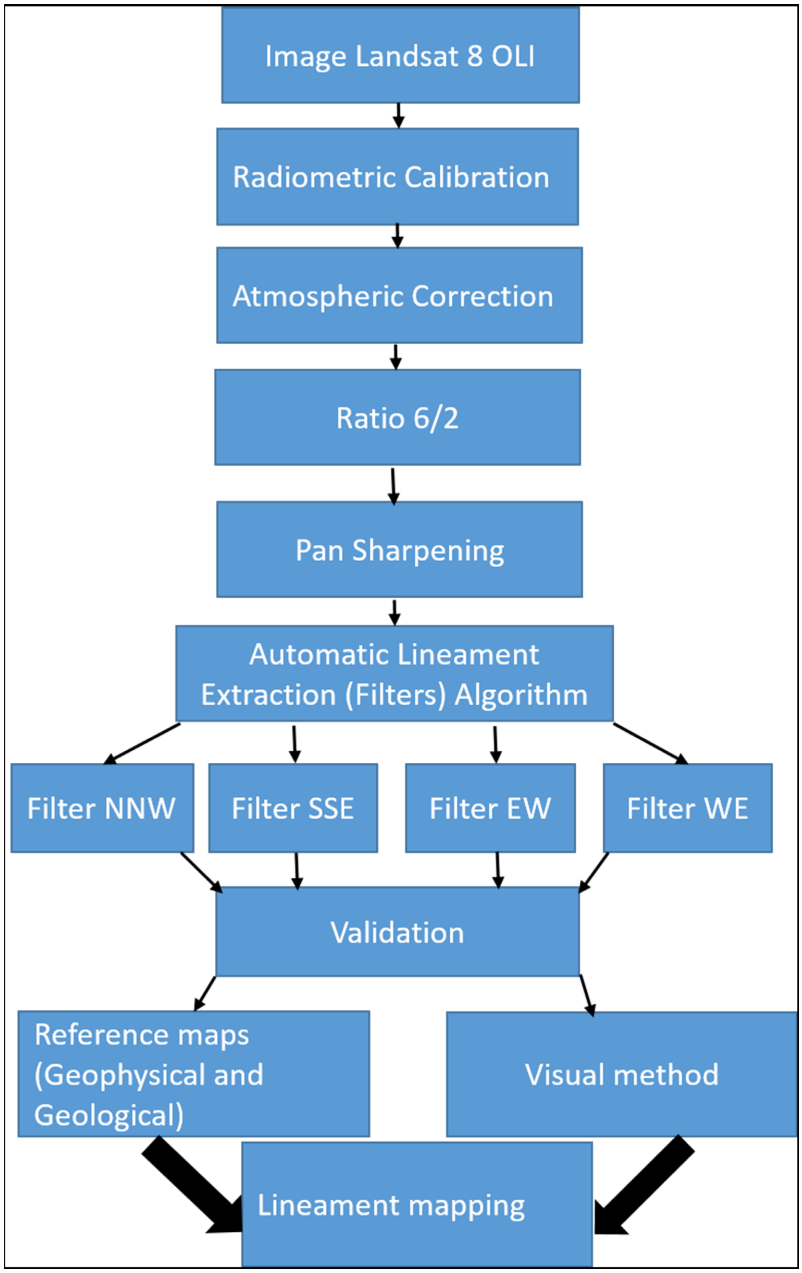

Figure 9. Flowchart showing the main steps of the methodology lineament extraction and validation approach.

processing, to enhance the visibility of lineaments in the images. The main purpose is to identify lineaments with possible structural origins. After several attempts using different image processing techniques, classifications and color composite images, we concluded that linear structures are more visible in the 6/2 band ratio images, the choice is also supported by other studies [66]. Hence, the ratio of 6/2 image was sharpened and directional filters were applied. Directional filters improve lineaments' perception by producing an optical shadow effect adjusted on the image as if it was enlightened by grazing light [67]. Besides, those filters enhance the detection of lineaments, which are not advantaged by the illumination source

[68]. We used Sobel operators, widely utilized for lineament extraction and edge detection [69], to enhance the lineaments automatically extracted from directional filters. Sobel filters consist of a selective variety of directional filters using a pair of convolution matrix of 3 × 3, one of them is the other mask rotated by 90˚ (**Table 2**), and is determined based on the distance from the central pixel. In this study, the image used for the filtering is Ratio 6/2.

Table 2. Sobel filters.

3 × 3 Sobel Matrix											
NNW-SSE			SSE-NNW			E-W			W-E		
−0.7	0.25	1.22	0.7	−0.25	−1.2	1	1	1	−1	−1	−1
−0.96	0	0.96	0.96	0	−1	0	0	0	0	0	0
−1.22	−0.3	0.7	1.22	0.25	−0.7	−1	−1	−1	1	1	1

From these directional filter images, the lineaments are automatically extracted, however, the result is not definitive, the work is still incomplete and a visual method must be used before reaching the next step of confirmation and validation. After enhancing the edges by directional filtering, we opted for visual inspection [72] [73]. This method allows choosing the significant lineaments of structural origin. Validation of fractures consists mainly of eliminating linear structures related to different parameters (e.g. ridgeline, shade, etc.), so we first compare our map of lineaments with geophysical and pre-existing structural map of Oudiane Elkharoub.

The processed Landsat 8 data were done using ENVI 5.3, QGIS 3.32 and ARGIS 10.8.

5. Results

5.1. Mineral Alteration

The regions of interest corresponding to these pixels are presented by special colors and were overlaid by ASTER grayscale imagery. Aster data after spectral processing by application of MNF, PPI, and n-d visualization has given endmembers, which yield very good results for classification and mapping.

The extracted index alteration minerals of sulfur, illite, kaolinite, alunite, chlorite, epidote, hematite and calcite were used for mineral detection by using the spectral angle mapping SAM algorithm. argillic index minerals have similar spectral features and are detectable by a low absorption feature in band 5 and stronger absorption in band 6, and epidote group minerals show absorption in band 8 (ASTER data). These spectral features are used for the detection of the target minerals.

The result of the SAM in this research shows that the yellow color index (**Figure 10**, **Figure 11**) represents the distribution of sulfur as a key mineral and indicator of hydrothermal alteration, kaolinite (blue), illite (red), alunite (purple), chlorite (green), epidote (sky blue), calcite (pink) and (maroon) illustrates hematite

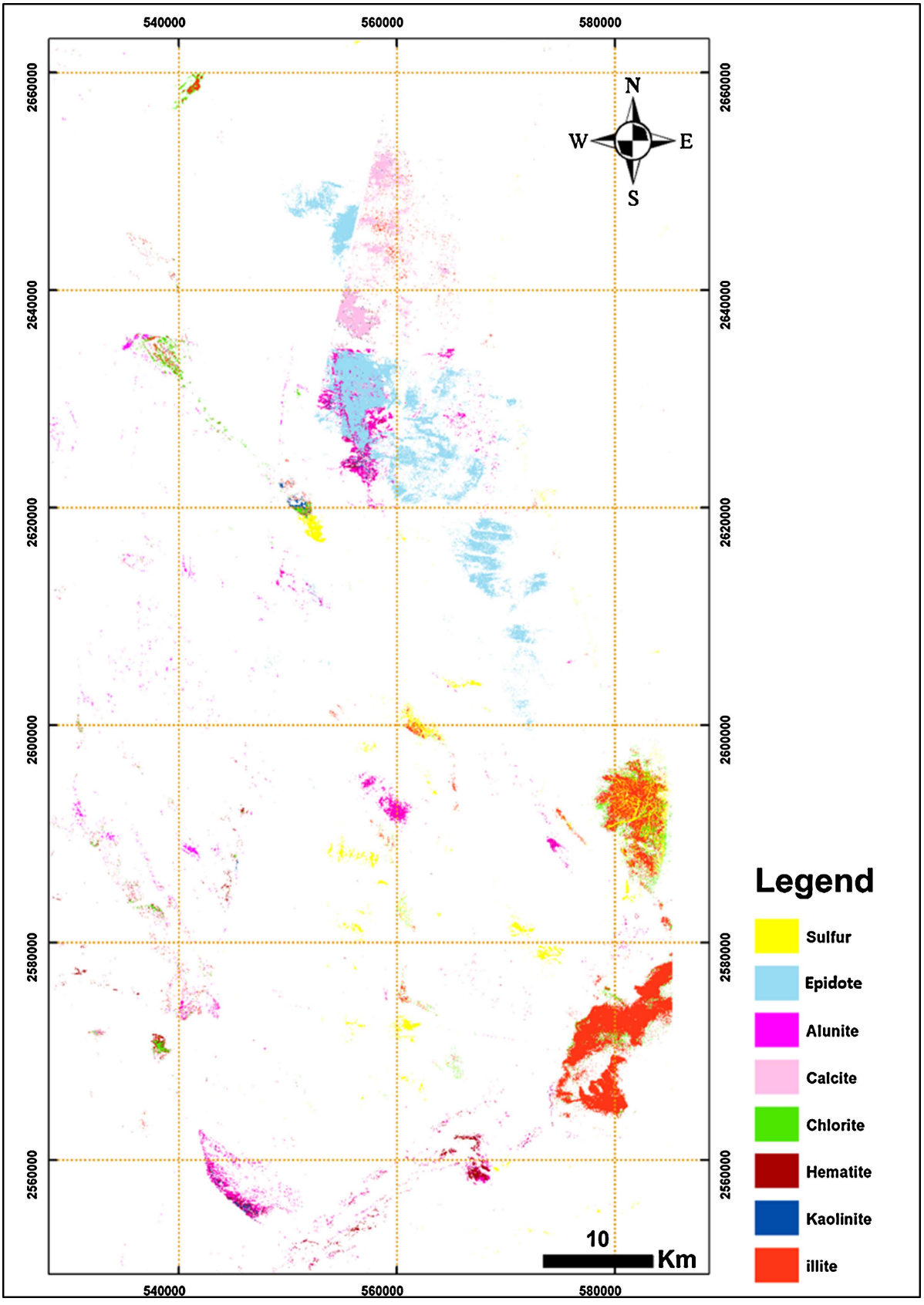

Figure 10. Spatiomap of mineral alteration in Oudiane Elkharoub area.

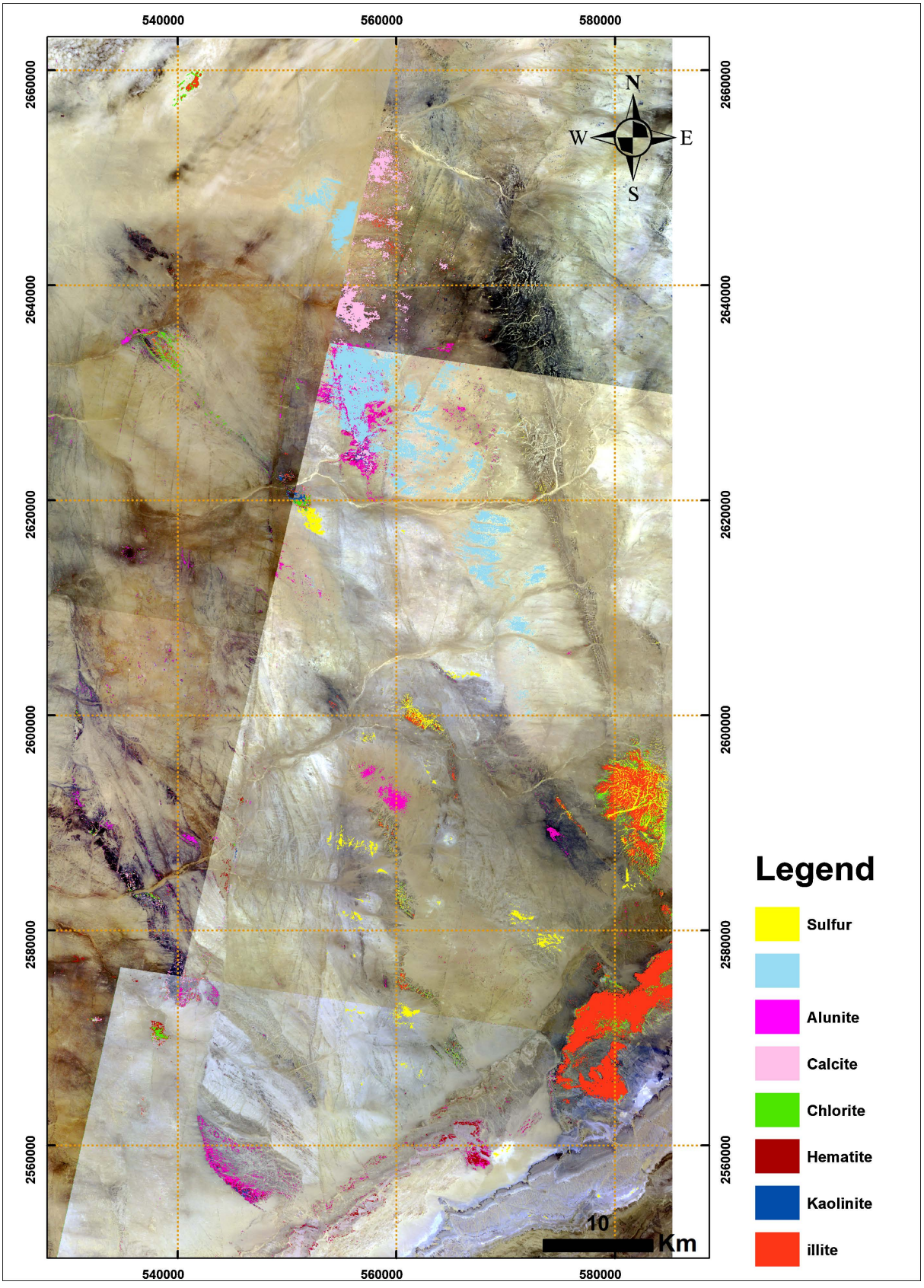

Figure 11. Spatiomap of mineral alteration in Oudiane Elkharoub area plotted on setalite image.

alteration (Figure 10, Figure 11) superimposed on the Birimian mafic rocks and granite, mostly in the southern, southeast and northeast part of Oudiane Elkharoub area.

There is a good matching between the sulfur alteration, chlorite, illite, kaolinite alteration and the significant spatial distribution of various anomalies of precious and base metal in Oudiane Elkharoub area.

5.2. Lineament Extraction

Results reveal the existence of more than 500 lineaments (Figure 12(a)-(d), Figure 13). The length of structures varies from few meters to few kilometers. Compared to materials used for validation, the number of highlighted structures within the area is more important in this study than the number of linear structures in geological, geophysical and structural maps, made based on fieldwork. Mapped lineaments generally correspond to fractures and faults, mainly related to intrusive and volcanic outcrops. Recorded structures in the geological maps and geophysical of Oudiane Ekharoub are quite the same, although, sometimes, the superimposition is conveyed through several segments and the result is spoiled.

This imperfection might be due to satellite images' spatial resolution (30 m) or lineaments' invisibility in these areas. The validation process of the outputs proves that coupling automatic extraction and visual interpretation methods give better results.

Oudiane Elkharoub structural and geophysical map show quite a good correlation of structures with what was obtained from the processing methods. Despite of the map, features are represented as huge faults and structures, trend and localization of the lineaments are respected in our generated map, with slight differences, yet very logical and acceptable. In fact, structures are represented as several aligned segments with the same direction (Figure 13).

Although the good results show a matching correlation with the structural map, we also note an anomalies correlation of some other features, which is when areas are covered with vegetation and the satellite images are unable to give accurate responses.

Geological maps of the studied area indicate the presence of several lineaments represented as faults and strike-slip faults. The density of lineaments in geological and geophysical maps and our generated map is identical. The trends of lineaments are globally coherent and consistent. However, structures in geological maps are sometimes shifted, probably because of projection systems' differences and induced errors. These results are therefore highly correlated with the faults' distribution depicted in structural and geological maps, with respect to remarks mentioned above.

6. Discussion and Field Verification

6.1. Mineral Alteration

In this study, several image-processing methods were utilized for ASTER imagery

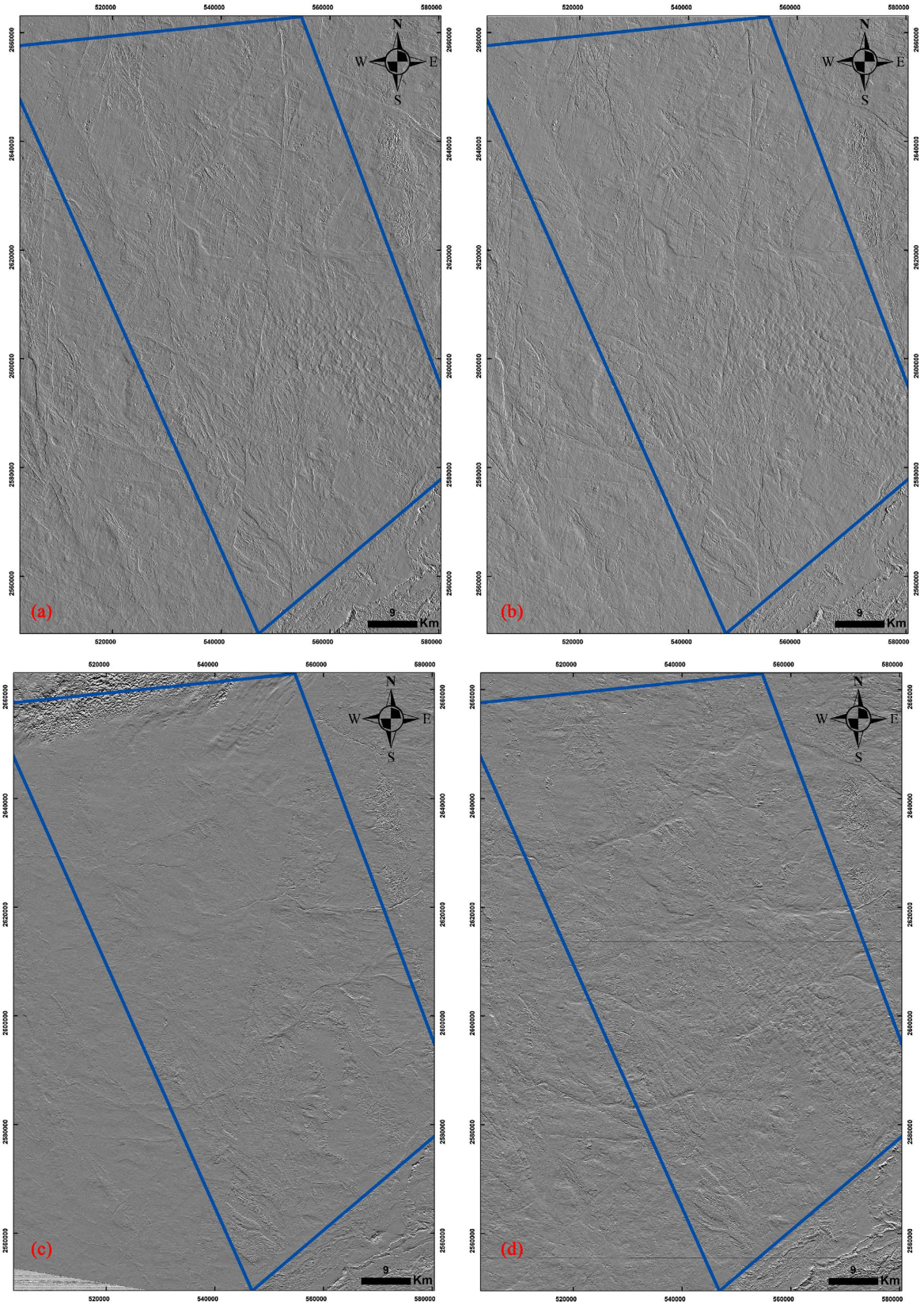

Figure 12. Example of different directional filters applied on the Oudiane Elkharoub area. (a) NNW-SSE, (b) SSE-NNW, (c) E-W, (d) W-E.

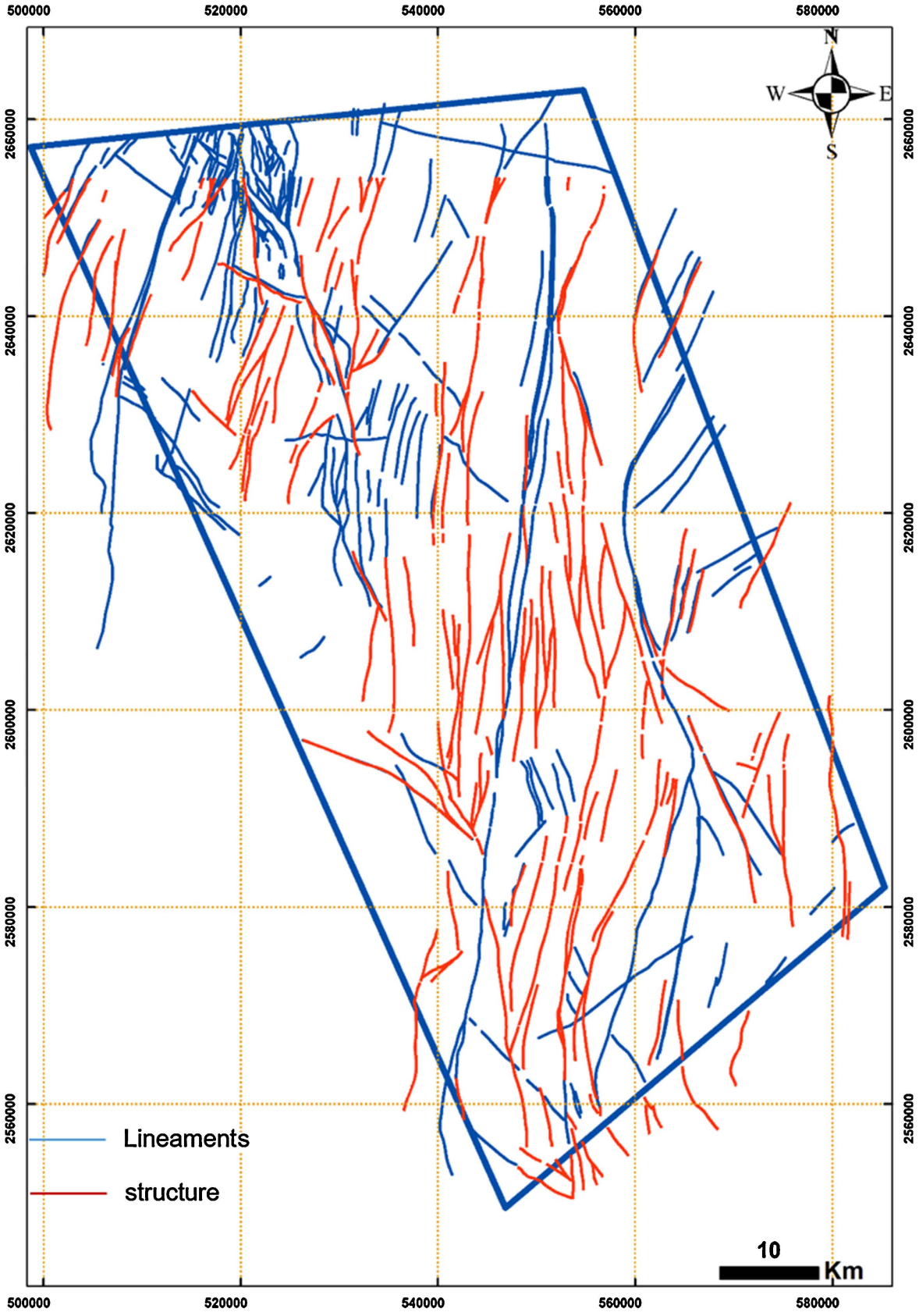

Figure 13. Lineaments maps with principal trends (NNW-SSE, SSE-NNW, E-W, and W-E).

including mixture tuned matched filtering, Spectral Angle Mapping, relative absorption band depth, band ratio, and principal component analysis. The imagery results show extensive alteration, which is expected, based on the good potential of mineralization in the Oudiane Elkharoub. By comparison, of these methods, the results show all applied algorithms provide identical locations for sulfur, kaolinite, chlorite, epidotic, hematite, illite, calcite and alunite alteration zones. We conclude that the utilized methods are adept at detection of mineral distribution at a large scale.

An overlay of alteration zones on the geological map in the studied area shows there is good correspondence between geology of the area studied and the distribution of alteration, which confirm our second hypothesis. For example, sulfur, chlorite and kaolinite alteration as shown in **Figure 10** and **Figure 11**, agrees with an outcrop diorite amphibolite in the southeast ant eastern of Oudiane Elkharoub. Alunite alteration is mostly tied to volcanic rocks. Thus, our results show that specific geological units in the study area correspond with specific alteration zones. Hydrothermal alteration is one of the main lines of evidence for identification of mineralization types such as gold, silver, lead, deposits, massive sulfide, iron oxide gold and copper deposits, and disseminated deposits.

The obtained imagery processing of hydrothermal alteration in this study has demonstrated the ability of ASTER to provide information on alteration mapping, which is valuable for mineral prospecting and exploration activities.

The hydrothermal alteration system in the Oudiane Elkharoub area is comparable to other global examples. Various techniques including minimum noise transformation, pixel purity index and matched filter processing were used to process ASTER data, which allowed for identification of sulfur, chlorite, kaolinite, calcite, illite, alunite and hematite alterations zones in the Oudiane Elkharoub area.

Obtained results were compared with field geology observation (**Figure 14**). Mineral alterations have been determined in studied area and both results confirm each other. Ten samples were collected for XRD studies that have confirmed mineral alterations and several of them is depicted in **Figure 15**. Sixty-six samples were collected for XRF analyses and sixteen samples for ICP-MS, which they have verified mineral alterations.

6.2. Lineament Extraction

During the last few decades, remote sensing has proven its effectiveness in every branch of geology, particularly in structural geology, tectonics, lithological mapping, and hydrothermal alteration among others. Lineament is a geological feature that includes faults, fractures, joints, and lithological boundaries. These structures can predominantly be determined from diverse remote sensing data sources and techniques. As such, the determination of geological lineaments allows the sufficient exploration of mineral deposits associated with hydrothermal alterations and magmatic processes. In addition, the lineaments can act as the influencing factors of mineral deposits potentiality, natural hazard assessment, including

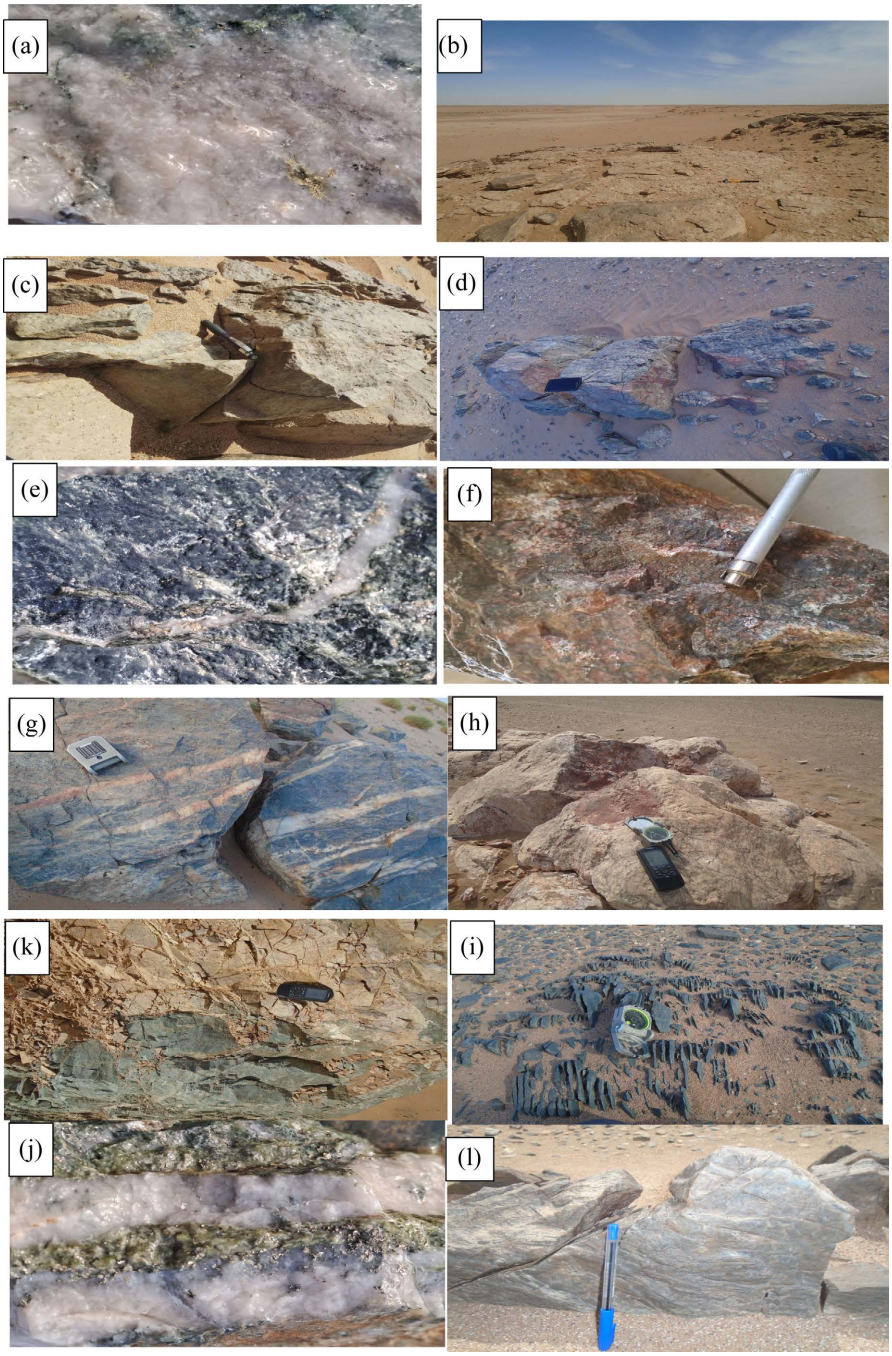

Figure 14. Field photographs showing gold with sulfur (a), calcite (b), albite (c), hematite (d), chlorite (e), hematite (f), biotite silice (g), quartz (h), epidote (k), chlorite, biotite (i), silice (j), and silica (l) in the Oudiane Elkharoub area.

earthquakes and seismicity, and land sliding.

Conventional geological lineament methodology is time-consuming and expensive. On the other hand, conventional approaches are challenging to apply due to the physical/geographical condition of the region of study. Remotely sensed mapping of geological lineaments leads to determine the faults, and their tectonic implication is the substitution of conventional methods. Manual geological

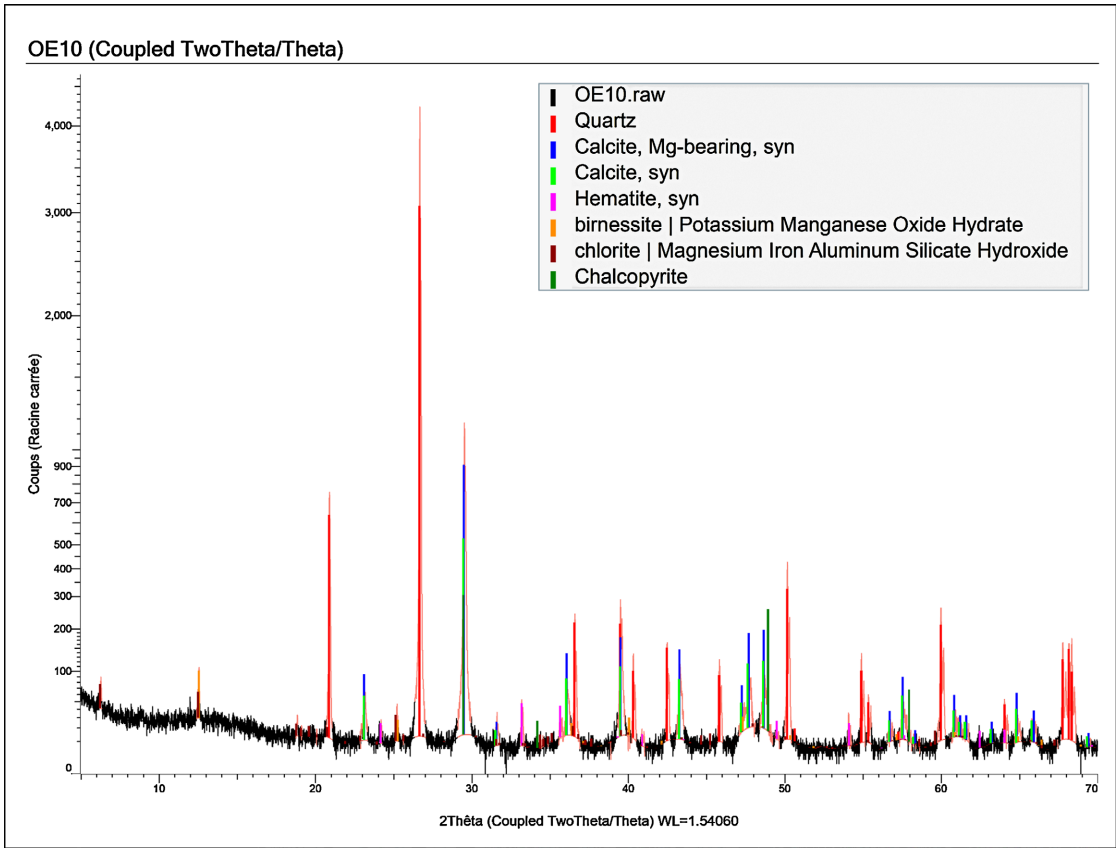
OE10 (Coupled TwoTheta/Theta)
OE10.raw
Quartz
Calcite, Mg-bearing, syn
Calcite, syn
Hematite, syn
birnessite | Potassium Manganese Oxide Hydrate
chlorite | Magnesium Iron Aluminum Silicate Hydroxide
Chalcopyrite
Coups (Racine carrée)
2Thêta (Coupled TwoTheta/Theta) WL=1.54060

(a)

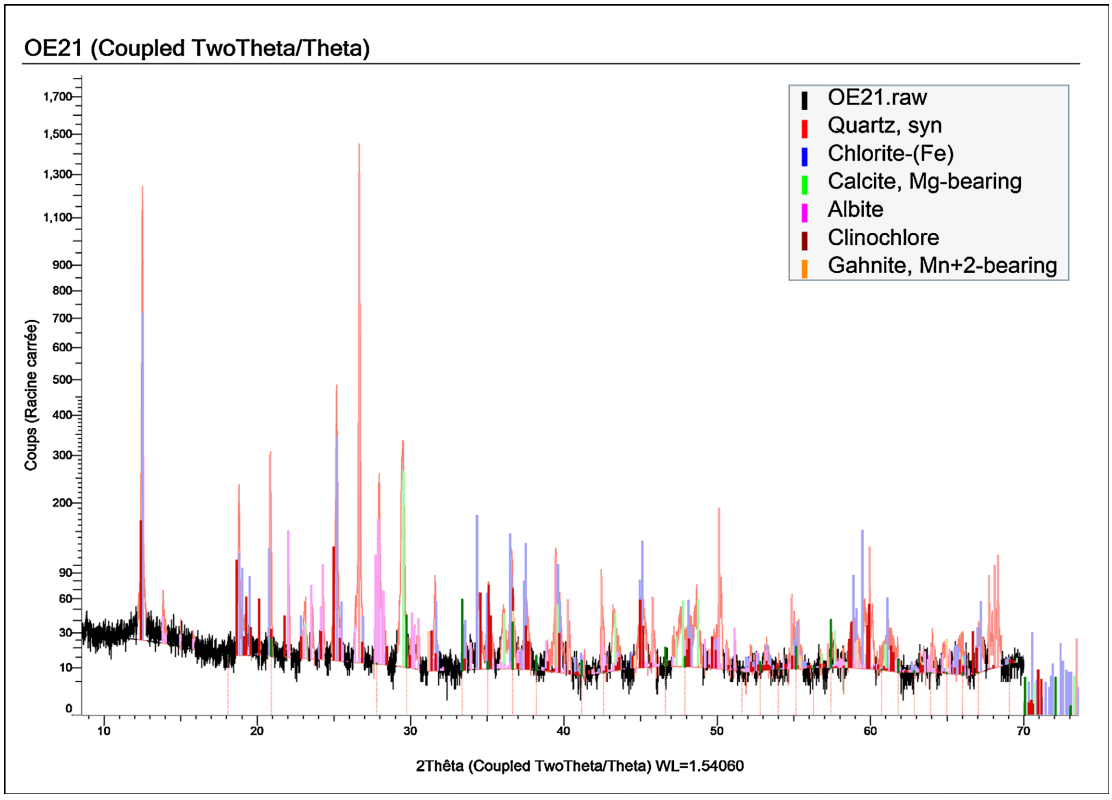
OE21 (Coupled TwoTheta/Theta)
OE21.raw
Quartz, syn
Chlorite-(Fe)
Calcite, Mg-bearing
Albite
Clinochlore
Gahnite, Mn+2-bearing
Coups (Racine carrée)
2Thêta (Coupled TwoTheta/Theta) WL=1.54060

(b)

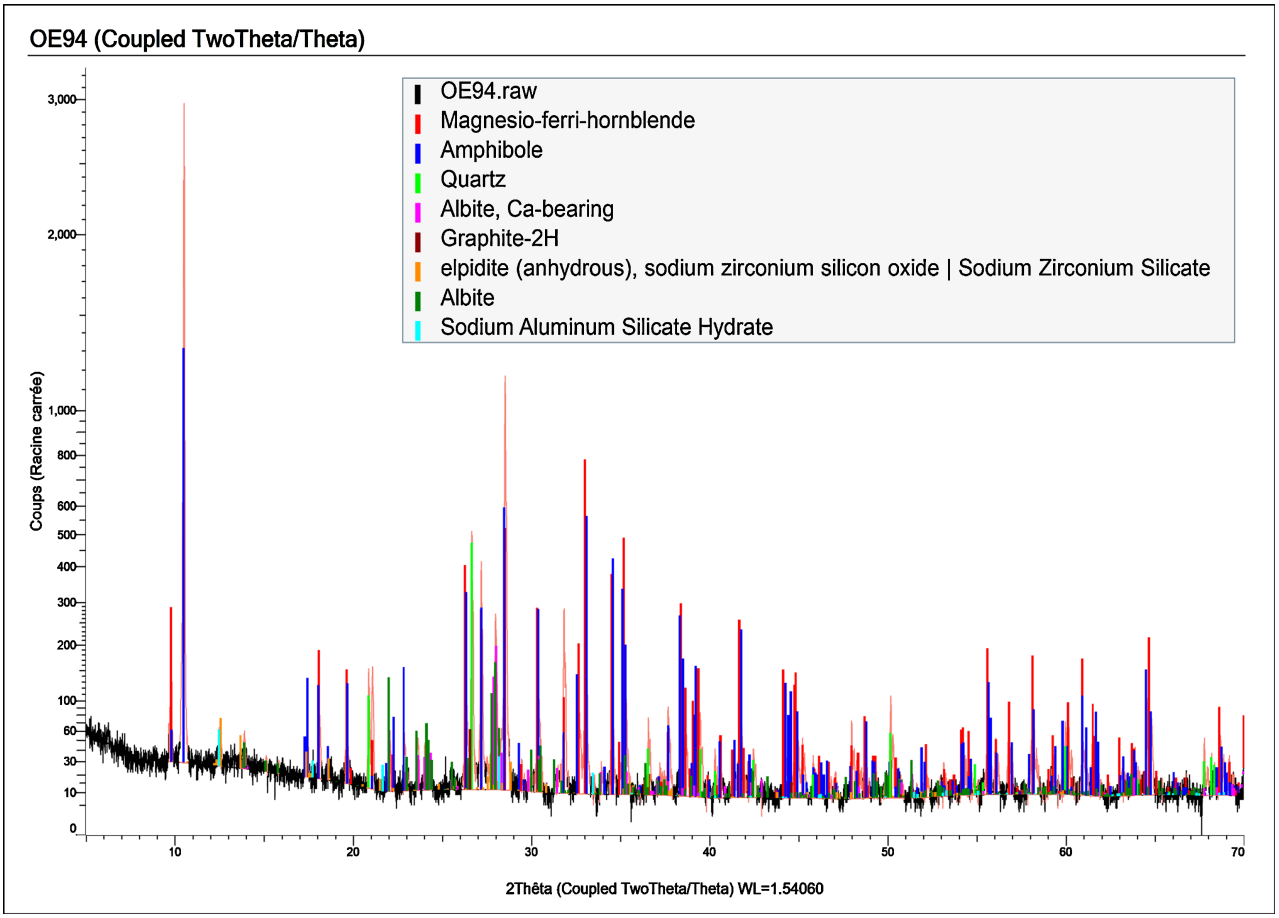

(c)

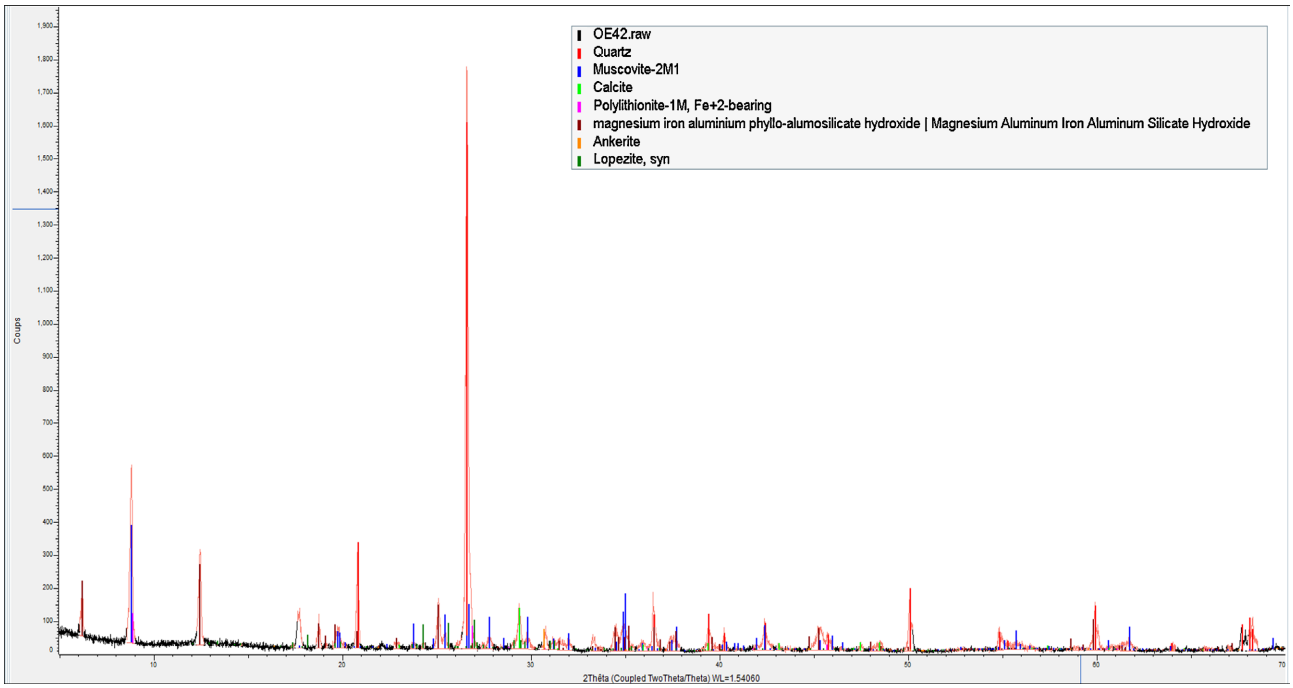

(d)

Figure 15. DRX result for samples: (a) 0E10, (b) OE 21, (c) OE94 and (d) OE42 showing the mineral composition of some samples.

extraction is carried out on the computer screen or hard copies. The growth of technology has changed the photo interpretation operation from the early usage of the stereoscope and transparent overlays to a very fast computer screen with high-definition resolution displays. Manual geological lineament extraction is directly associated with the interpreter's skill and experience and the remote sensing data. As the lineaments, the sharp and distinctive line between adjacent regions of an image, are seen by human eyes, therefore, an image with coarse resolution and noise resulting blur decreasing the chance of appearing edges and/or linear features. To overcome this visual distinctiveness, different edge enhancement and filtering are applied. Ramli *et al.* [74] stated the manual lineament extraction subjectivity as a controversial result, reproductivity, and positioning in highly vegetated or wide valleys. The authors also described the final lineament map as integrated with the results from multiple observers to minimize the subjectivity.

Therefore, it is suggested to generate a significantly tectonic-geological lineament map using the integration of automatic and manual techniques. The generated map should be compared and verified with the previously every possible mapped structure. In case of possibilities, integration of geophysical data and extensive fieldworks is suggested. Geological lineaments are extracted for various purposes such as tectonic faults, hydrogeology, and earthquakes. In each case, specific validation and accuracy assessment is applied. In targeting the tectonic faults, the generated geological faults are validated using geophysical data or previously mapped faults. The generated map is suggested to be validated with the land deformation deduced by the tectonic activities to get the confidential result. The tectonic activity or land deformation must indicate an active fault. Therefore, geological lineaments' distribution might be observed in an area with high activity of tectonism and land deformation.

The comparison of the existing geophysical (**Figure 16**) and geological data showed a good matching with the lineaments processed from the remote sensing data.

According to the results of the samples taken from Oudiane Elkharoub area, the existing mineralization is controlled by the structure (shear zone) that intersects the different lithology, indeed, hydrothermal fluids would use the shear zone along with faults and fractures as pathways for their circulation and for the mineralization's precipitation.

7. Conclusions

Classical geological mapping based on the field missions is a job that is long, complex, tedious and very expensive. The digital extraction method of geological information using remote sensing not only offers better readability, but also means of observing geological elements in several aspects through various treatments. These different assets allow a map to be as close as possible to the reality, which fieldwork must nevertheless reinforce.

The different treatments carried out on the ASTER and Landsat 8 OLI images

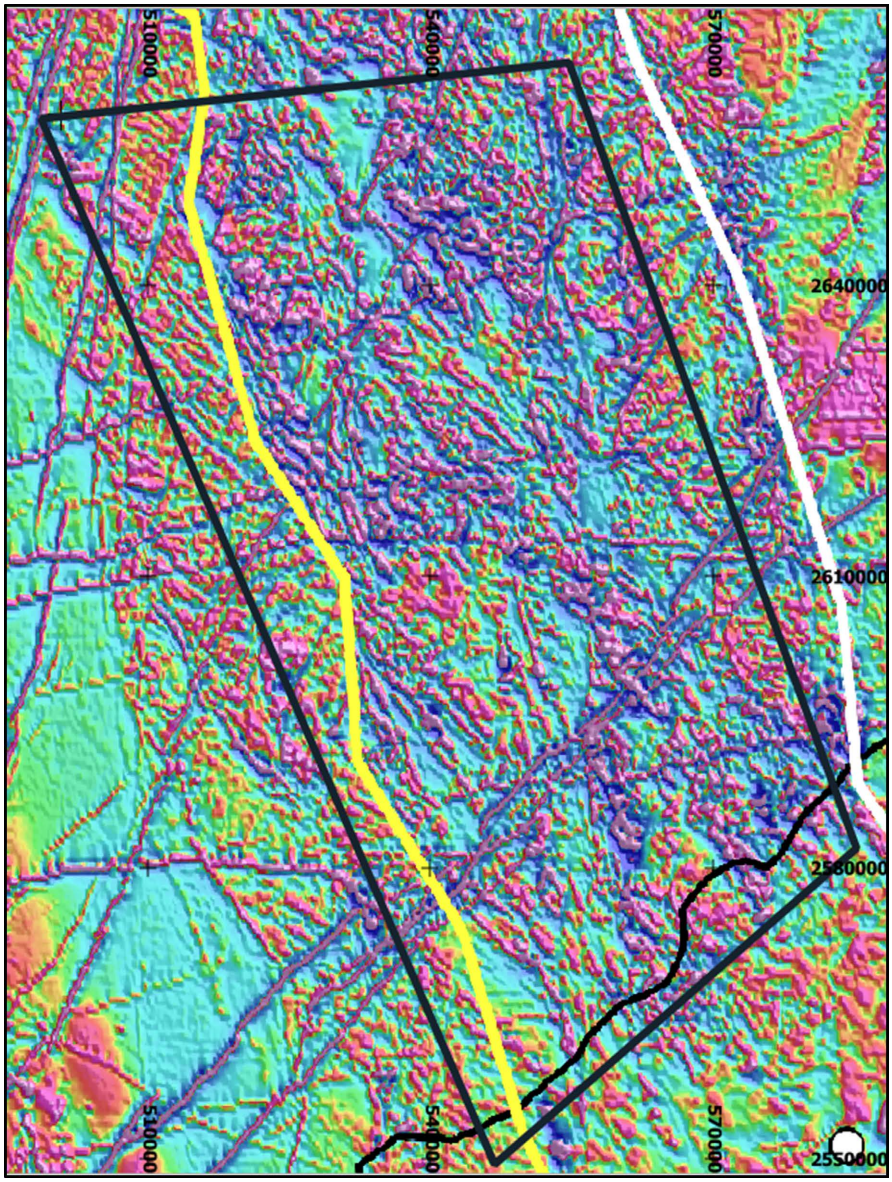

Figure 16. Geophysical map of Oudiane Elkharoub after [56].

as part of this work made it possible to extract mineral alteration and lineaments in Oudiane Elkharoub area. In addition, remote sensing can be of great benefit in this regard. The reliability of remote sensing is simultaneously confirmed by the field investigation and samples analysis. Ultimately, this study confirms a good identical between the extracted geological information using remote sensing in Oudiane Elkharoub and the analysis carried out on the samples taken from the field and the field verification. This study should contribute to help to revitalize the mining sector.

The main considerations for remote sensing applications in mineral resource mapping are that reconnaissance lithological mapping is usually the first step of mineral resource mapping project and alteration mapping to deduce the information about the possible mineral resource. Mineral deposits are commonly associated

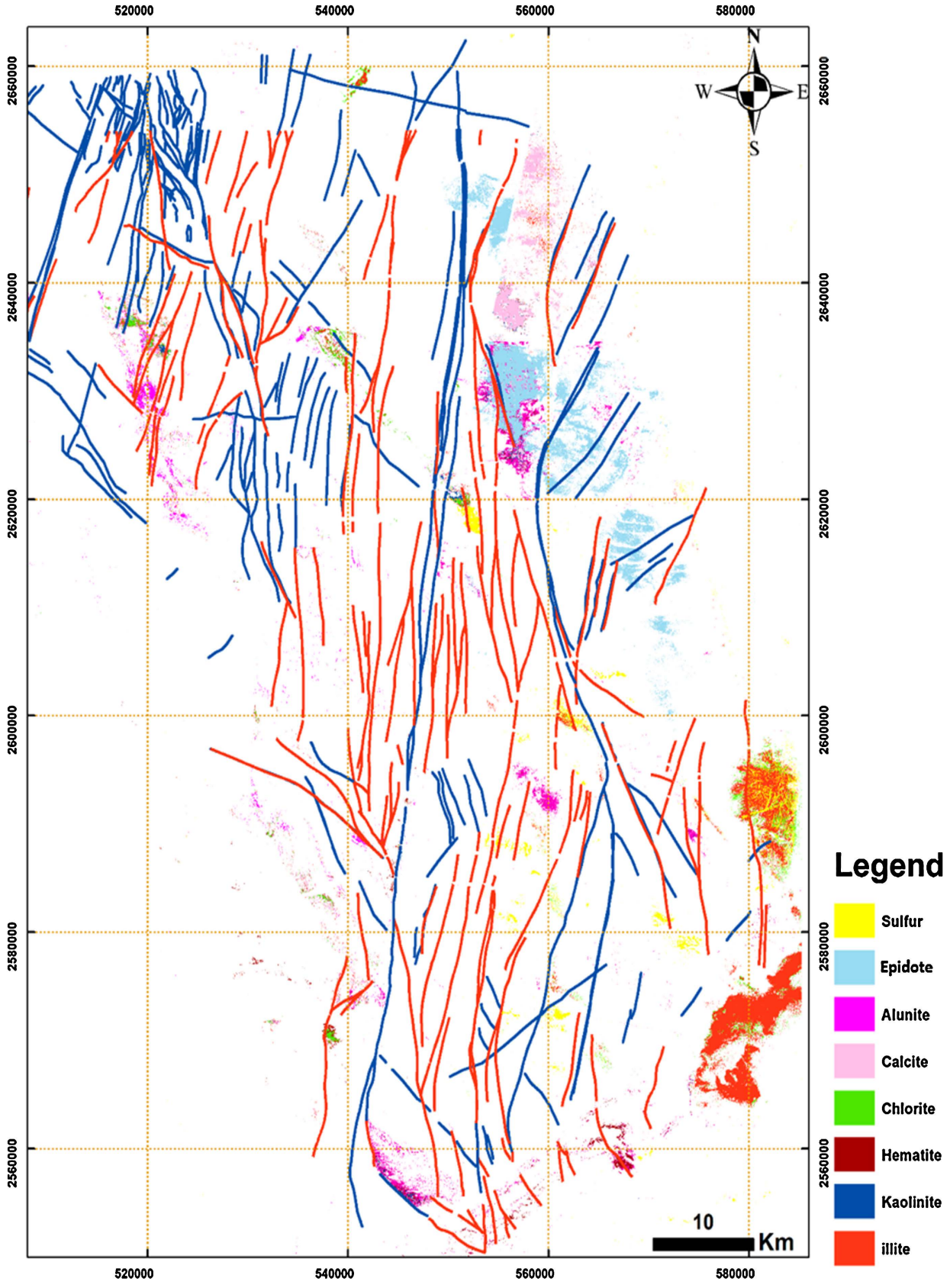

Figure 17. Final extracted mineral alteration map from ASTER and lineament extracted from Landsat 8 in Oudiane Elkharoub.

with hydrothermal alteration of surrounding rocks, lineament extraction and finally coming to exploration stage, it is clear that the remote sensing data gathered has to be integrated with other geoscience data like mineralogical and geophysical data.

In this study, eight mineral alteration zones are recognized in the Oudiane Elkharoub area: sulfur, chlorite, epidote, alunite, calcite, kaolinite, illlite and hematite. In addition to mineral alteration, more than 500 lineaments were extracted. Our research has highlighted the advantage of using low-cost and reliable remote sensing techniques in prospecting mineral sources.

Final extracted hydrothermal alterations map from ASTER data by SAM method and lineament extraction from Landsat 8 data in Oudiane Elkharoub area is demonstrated in **Figure 17**. Recognized alteration zones have been confirmed by field geology observations, X-Ray Florescence (XRF) and X-Ray Diffraction (XRD) analyses. All evidence and experiments have displayed that SAM is an adequate and commodious technique for separation and recognition of hydrothermal alterations minerals.

Acknowledgements

This study is part of a Ph.D. thesis of the first author (HM, in progress) under the supervision of Dr. Zouhir Baroudi and Dr. Malika Adjour (Hassan II University, Casablanca). Our thanks go to Mr. Mohamed Raji, Mr. Zouhair Baroudi and Mme. Malika Adjour for the recommendations and availability. We sincerely thank the reviewers and assigned editor of this paper.

Conflicts of Interest

The authors declare no conflicts of interest regarding the publication of this paper.

References

[1] Ahmadi, H. and Uygucgil, H. (2021) Targeting Iron Prospective within the Kabul Block (SE Afghanistan) via Hydrothermal Alteration Mapping Using Remote Sensing Techniques. *Arabian Journal of Geosciences*, **14**, Article No. 183. https://doi.org/10.1007/s12517-020-06430-3

[2] Testa, F., Villanueva, C., Cooke, D. and Zhang, L. (2018) Lithological and Hydrothermal Alteration Mapping of Epithermal, Porphyry and Tourmaline Breccia Districts in the Argentine Andes Using ASTER Imagery. *Remote Sensing*, **10**, Article 203. https://doi.org/10.3390/rs10020203

[3] Mathieu, L. (2018) Quantifying Hydrothermal Alteration: A Review of Methods. *Geosciences*, **8**, Article 245. https://doi.org/10.3390/geosciences8070245

[4] Goetz, A.F.H., Rock, B.N. and Rowan, L.C. (1983) Remote Sensing for Exploration; an Overview. *Economic Geology*, **78**, 573-590. https://doi.org/10.2113/gsecongeo.78.4.573

[5] Poormirzaee, R. and Oskouei, M.M. (2009) Detection Minerals by Advanced Spectral Analysis in ETM+ Imagery. *Proceeding of 7th Iranian Student Conference Mining Engineering*, Tabriz, 22 September 2009, 111-119.

[6] Sabins, F.F. (1999) Remote Sensing for Mineral Exploration. *Ore Geology Reviews*, **14**, 157-183. https://doi.org/10.1016/s0169-1368(99)00007-4

[7] Abrams, M.J., Brown, D., Lepley, L. and Sadowski, R. (1983) Remote Sensing for Porphyry Copper Deposits in Southern Arizona. *Economic Geology*, **78**, 591-604. https://doi.org/10.2113/gsecongeo.78.4.591

[8] Sabins, F.F. (1997) Remote Sensing Strategies for Mineral Exploration. In: Rencz, A.E., Ed., *Remote Sensing for the Earth Sciences*, John Wiley & Sons, 375-447.

[9] Ninomiya, Y. (2003) Advanced Remote Lithologic Mapping in Ophiolite Zone with ASTER Multispectral Thermal Infrared Data. *IGARSS* 2003. 2003 *IEEE International Geoscience and Remote Sensing Symposium. Proceedings* (*IEEE Cat. No.*03*CH*37477), Toulouse, 21-25 July 2003, 1561-1563. https://doi.org/10.1109/igarss.2003.1294175

[10] Gabr, S., Ghulam, A. and Kusky, T. (2010) Detecting Areas of High-Potential Gold Mineralization Using ASTER Data. *Ore Geology Reviews*, **38**, 59-69. https://doi.org/10.1016/j.oregeorev.2010.05.007

[11] Tangestani, M.H. and Moore, F. (2000) Iron Oxide and Hydroxyl Enhancement Using the Crosta Method: A Case Study from the Zagros Belt, Fars Province, Iran. *International Journal of Applied Earth Observation and Geoinformation*, **2**, 140-146. https://doi.org/10.1016/s0303-2434(00)85007-2

[12] Mia, B. and Fujimitsu, Y. (2012) Mapping Hydrothermal Altered Mineral Deposits Using Landsat 7 ETM+ Image in and around Kuju Volcano, Kyushu, Japan. *Journal of Earth System Science*, **121**, 1049-1057. https://doi.org/10.1007/s12040-012-0211-9

[13] Yajima, T. (2014) ASTER Data Analysis Applied to Mineral Resource Exploration and Geological Mapping. Ph.D. Thesis, Nagoya University.

[14] Abdelkareem, M., Kamal El-Din, G.M. and Osman, I. (2018) An Integrated Approach for Mapping Mineral Resources in the Eastern Desert of Egypt. *International Journal of Applied Earth Observation and Geoinformation*, **73**, 682-696. https://doi.org/10.1016/j.jag.2018.07.005

[15] Zhang, X., Pazner, M. and Duke, N. (2007) Lithologic and Mineral Information Extraction for Gold Exploration Using ASTER Data in the South Chocolate Mountains (California). *ISPRS Journal of Photogrammetry and Remote Sensing*, **62**, 271-282. https://doi.org/10.1016/j.isprsjprs.2007.04.004

[16] Azizi, H., Tarverdi, M.A. and Akbarpour, A. (2010) Extraction of Hydrothermal Alterations from ASTER SWIR Data from East Zanjan, Northern Iran. *Advances in Space Research*, **46**, 99-109. https://doi.org/10.1016/j.asr.2010.03.014

[17] Guha, A., Singh, V.K., Parveen, R., Kumar, K.V., Jeyaseelan, A.T. and Dhanamjaya Rao, E.N. (2013) Analysis of ASTER Data for Mapping Bauxite Rich Pockets within High Altitude Lateritic Bauxite, Jharkhand, India. *International Journal of Applied Earth Observation and Geoinformation*, **21**, 184-194. https://doi.org/10.1016/j.jag.2012.08.003

[18] Abrams, M. and Hook, S.J. (1995) Simulated Aster Data for Geologic Studies. *IEEE Transactions on Geoscience and Remote Sensing*, **33**, 692-699. https://doi.org/10.1109/36.387584

[19] Mars, J.C. and Rowan, L.C. (2006) Regional Mapping of Phyllic- and Argillic-Altered Rocks in the Zagros Magmatic Arc, Iran, Using Advanced Spaceborne Thermal Emission and Reflection Radiometer (ASTER) Data and Logical Operator Algorithms. *Geosphere*, **2**, 161-186.

[20] Crósta, A.P., De Souza Filho, C.R., Azevedo, F. and Brodie, C. (2003) Targeting Key Alteration Minerals in Epithermal Deposits in Patagonia, Argentina, Using ASTER Imagery and Principal Component Analysis. *International Journal of Remote Sensing*,

24, 4233-4240. https://doi.org/10.1080/0143116031000152291

[21] Galvão, L.S., Almeida-Filho, R. and Vitorello, Í. (2005) Spectral Discrimination of Hydrothermally Altered Materials Using ASTER Short-Wave Infrared Bands: Evaluation in a Tropical Savannah Environment. *International Journal of Applied Earth Observation and Geoinformation*, **7**, 107-114. https://doi.org/10.1016/j.jag.2004.12.003

[22] Yamaguchi, Y. and Naito, C. (2003) Spectral Indices for Lithologic Discrimination and Mapping by Using the ASTER SWIR Bands. *International Journal of Remote Sensing*, **24**, 4311-4323. https://doi.org/10.1080/01431160110070320

[23] Abdelkareem, M. and El-Baz, F. (2017) Characterizing Hydrothermal Alteration Zones in Hamama Area in the Central Eastern Desert of Egypt by Remotely Sensed Data. *Geocarto International*, **33**, 1307-1325. https://doi.org/10.1080/10106049.2017.1325410

[24] Zadeh, M.H., Tangestani, M.H., Roldan, F.V. and Yusta, I. (2014) Mineral Exploration and Alteration Zone Mapping Using Mixture Tuned Matched Filtering Approach on ASTER Data at the Central Part of Dehaj-Sarduiyeh Copper Belt, SE Iran. *IEEE Journal of Selected Topics in Applied Earth Observations and Remote Sensing*, **7**, 284-289. https://doi.org/10.1109/jstars.2013.2261800

[25] Pour, A.B. and Hashim, M. (2014) Integrating PALSAR and ASTER Data for Mineral Deposits Exploration in Tropical Environments: A Case Study from Central Belt, Peninsular Malaysia. *International Journal of Image and Data Fusion*, **6**, 170-188. https://doi.org/10.1080/19479832.2014.985619

[26] Crowley, J.K., Brickey, D.W. and Rowan, L.C. (1989) Airborne Imaging Spectrometer Data of the Ruby Mountains, Montana: Mineral Discrimination Using Relative Absorption Band-Depth Images. *Remote Sensing of Environment*, **29**, 121-134. https://doi.org/10.1016/0034-4257(89)90021-7

[27] Rowan, L.C. and Mars, J.C. (2003) Lithologic Mapping in the Mountain Pass, California Area Using Advanced Spaceborne Thermal Emission and Reflection Radiometer (ASTER) Data. *Remote Sensing of Environment*, **84**, 350-366. https://doi.org/10.1016/s0034-4257(02)00127-x

[28] Rowan, L.C., Goetz, A.F.H. and Ashley, R.P. (1977) Discrimination of Hydrothermally Altered and Unaltered Rocks in Visible and near Infrared Multispectral Images. *Geophysics*, **42**, 522-535. https://doi.org/10.1190/1.1440723

[29] Gupta, R.P. (2003) Remote Sensing Geology. 2nd Edition, Springer-Verlag. https://books.google.com/books?hl=en&lr=&id=lERADwAAQBAJ&oi=fnd&pg=PR9&dq=Gupta+RP.+Remote+sensing+Geology.+2nd+ed.+Berlin:+Springer&ots=p5_nwxpa3_&sig=YAVbd9a_uZv4doH9Y2AMBjy2nSI#v=onepage&q=Gupta%20RP.%20Remote%20sensing%20Geology.%202nd%20ed.%20Berlin%3A%20Springer&f=false

[30] Hezarkhani, A. (2006) Hydrothermal Evolution of the Sar-Cheshmeh Porphyry Cu-Mo Deposit, Iran: Evidence from Fluid Inclusions. *Journal of Asian Earth Sciences*, **28**, 409-422. https://doi.org/10.1016/j.jseaes.2005.11.003

[31] Joly, A., Porwal, A., McCuaig, T.C., Chudasama, B., Dentith, M.C. and Aitken, A.R.A. (2015) Mineral Systems Approach Applied to GIS-Based 2D-Prospectivity Modelling of Geological Regions: Insights from Western Australia. *Ore Geology Reviews*, **71**, 673-702. https://doi.org/10.1016/j.oregeorev.2015.06.007

[32] Sun, T., Chen, F., Zhong, L., Liu, W. and Wang, Y. (2019) GIS-Based Mineral Prospectivity Mapping Using Machine Learning Methods: A Case Study from Tongling Ore District, Eastern China. *Ore Geology Reviews*, **109**, 26-49. https://doi.org/10.1016/j.oregeorev.2019.04.003

[33] Carranza, E.J.M., Hale, M. and Faassen, C. (2008) Selection of Coherent Deposit-Type Locations and Their Application in Data-Driven Mineral Prospectivity Mapping. *Ore Geology Reviews*, **33**, 536-558. https://doi.org/10.1016/j.oregeorev.2007.07.001

[34] Campos, L.D., de Souza, S.M., de Sordi, D.A., Tavares, F.M., Klein, E.L. and Lopes, E.C.D.S. (2017) Predictive Mapping of Prospectivity in the Gurupi Orogenic Gold Belt, North-Northeast Brazil: An Example of District-Scale Mineral System Approach to Exploration Targeting. *Natural Resources Research*, **26**, 509-534. https://doi.org/10.1007/s11053-016-9320-5

[35] Carranza, E.J.M. and Laborte, A.G. (2015) Data-Driven Predictive Mapping of Gold Prospectivity, Baguio District, Philippines: Application of Random Forests Algorithm. *Ore Geology Reviews*, **71**, 777-787. https://doi.org/10.1016/j.oregeorev.2014.08.010

[36] Podwysocki, M.H., Segal, D.B. and Jones, O.D. (1983) Mapping of Hydrothermally Altered Rocks Using Airborne Multispectral Scanner Data, Marysvale, Utah, Mining District. *Advances in Space Research*, **3**, 101-112. https://doi.org/10.1016/0273-1177(83)90109-6

[37] Tangestani, M.H. and Moore, F. (2002) Porphyry Copper Alteration Mapping at the Meiduk Area, Iran. *International Journal of Remote Sensing*, **23**, 4815-4825. https://doi.org/10.1080/01431160110115564

[38] Farrand, W.H. (1997) Identification and Mapping of Ferric Oxide and Oxyhydroxide Minerals in Imaging Spectrometer Data of Summitville, Colorado, U.S.A., and the Surrounding San Juan Mountains. *International Journal of Remote Sensing*, **18**, 1543-1552. https://doi.org/10.1080/014311697218269

[39] Spatz, D.M. (1997) Remote Sensing Characteristics of the Sediment- and Volcanic-Hosted Precious Metal Systems: Imagery Selection for Exploration and Development. *International Journal of Remote Sensing*, **18**, 1413-1438. https://doi.org/10.1080/014311697218205

[40] Neville, R.A., Sun, L. and Staenz, K. (2003) Detection of Spectral Line Curvature in Imaging Spectrometer Data. *SPIE Proceedings*, **5093**, 144-154. https://doi.org/10.1117/12.487342

[41] Akhavi, M.S., Webster, T.L. and Raymond, D.A. (2001) RADARSAT-1 Imagery and GIS Modeling for Mineral Exploration in Nova Scotia, Canada. *Geocarto International*, **16**, 57-64. https://doi.org/10.1080/10106040108542183

[42] Rocci, G. (1966) Essai d'interprétation des mesures géochronologique de la structure de l'Ouest africain. *Science Terre*, **10**, 3-4.

[43] Bessoles, B. (1977) Géologie de l'Afrique: Le craton ouest africain. *Bureau de Recherche de la Géologie et des Mines*, *Mémoire*, **88**, 403.

[44] Potrel, A. (1994) Evolution tectono-métamorphique d'un segment de croute continentale Archéenne. Exemple de l'Amsaga (R.I. Mauritanie), Dorsale Rgueibat. Ph.D. Thesis, Université de Rennes. https://theses.hal.science/tel-00675134/

[45] Traore, D.Y. (2017) Etude Metallogenique du district aurifère de Syama (Mali): Analyse comparative de gisement situes sur un même structure lithosphérique éburnéenne. Ph.D. Thesis, Université Paul Sabatier-Toulouse III. https://theses.hal.science/tel-01900948/

[46] Pitfield, *et al.* (2004) Geology of the West African Craton.

[47] Ennih, N. and Liégeois, J. (2008) The Boundaries of the West African Craton, with Special Reference to the Basement of the Moroccan Metacratonic Anti-Atlas Belt. *Geological Society*, *London*, *Special Publications*, **297**, 1-17. https://doi.org/10.1144/sp297.1

[48] Heron, K. (2016) Origine et évolution de la Ceinture Verte Mesarchéenne d'Aoueouat et la minéralisation aurifère associée. Ph.D. Thesis, Trinity College.

[49] Villeneuve, M. (2008) Review of the Orogenic Belts on the Western Side of the West African Craton: The Bassarides, Rokelides and Mauritanides. *Geological Society, London, Special Publications*, **297**, 169-201. https://doi.org/10.1144/sp297.8

[50] Kah, L.C., Bartley, J.K. and Teal, D.A. (2012) Chemostratigraphy of the Late Mesoproterozoic Atar Group, Taoudeni Basin, Mauritania: Muted Isotopic Variability, Facies Correlation, and Global Isotopic Trends. *Precambrian Research*, **200**, 82-103. https://doi.org/10.1016/j.precamres.2012.01.011

[51] Taib, M. (2012) The Mineral Industry of Mauritania. USGS Minerals Yearbook 2012 (Advance Release). https://books.google.com/books?hl=en&lr=&id=SkhxjpjwEq0C&oi=fnd&pg=SA28-PA7&dq=Taib,+M.,+2012.+The+Mineral+Industry+of+Mauritania,+USGS+Minerals+Yearbook+2012&ots=TLA0CCBUTP&sig=N6IlaVe7wZHky8vKMbXYK3lhNk4#v=onepage&q&f=false

[52] Taleb, O.A. (1994) Caractérisation pétrographique et géochimique du plutonisme birimien de la dorsale Reguibat (Mauritanie, Afrique de l'Ouest). Master's Thesis, Henri Poincaré University. https://hal.univ-lorraine.fr/tel-01747477

[53] Thieblemont, D., Lahondere, D., Goujou, C., Roger, J., Metour, J., Marchand, J., Gatta, B., O'Hadi, M., Diabira, F.B. and Thiam, B. (2003) Carte géologique a 1/200000 du Nord de la Mauritanie, 14 coupure. DMG, Ministère des Mine et de l'Industrie.

[54] Lahondere, D., Thieblemont, D., Goujou, J.C., Roger, J., Moussine-Pouchkine, A., Le Metour, J., Cocherie, A. and Guerrot, C. (2003) Notice explicative des cartes géologiques et gitologiques a 1/200000 et 1/500000 du Nord de la Mauritanie. Volume 1. DMG, Ministère des Mines et de l'Industrie.

[55] Lahondere, D., Rogger, J., Thieblemont, D., Goujou, J.C., Marchand, J., Bronner, G. and Le Metour, J. (2003) Notice explicative des cartes géologiques a 1/500000 du Nord de la Mauritanie, 9 coupures. DMG, Ministère des Mines et de l'Industrie.

[56] Finn, C.A. and Horton, J.D. (2012) A Ministère du pétrole, de l'énergie et des mines. U.S Geological Survey Administrative Report.

[57] Lepretre, *et al.* (2015) Geological Map Presenting the West African Craton, Centered on the Reguibat Shield.

[58] Green, A.A. and Craig, M.D. (1985) Analysis of Aircraft Spectrometer Data with Logarithmic Residuals. *Proceedings of the Airborne Imaging Spectrometer Data Analysis Workshop*, Pasadena, 8-10 April 1985, 111-119. https://ntrs.nasa.gov/api/citations/19860002169/downloads/19860002169.pdf

[59] Kruse, F.A., Lefkoff, A.B., Boardman, J.W., Heidebrecht, K.B., Shapiro, A.T., Barloon, P.J., *et al.* (1993) The Spectral Image Processing System (SIPS)—Interactive Visualization and Analysis of Imaging Spectrometer Data. *Remote Sensing of Environment*, **44**, 145-163. https://doi.org/10.1016/0034-4257(93)90013-n

[60] Boardman, W. and Kruse, F.A. (1994) Automated Spectra Analysis: A Geologic Example Using AVIRIS Data, North Grapevine on Geologic Remote Sensing. Environmental Research Institute of Michigan, 407-418.

[61] Lowell, J.D. and Guilbert, J.M. (1970) Lateral and Vertical Alteration-Mineralization Zoning in Porphyry Ore Deposits. *Economic Geology*, **65**, 373-408. https://doi.org/10.2113/gsecongeo.65.4.373

[62] Meyer, D., Siemonsma, D., Brooks, B. and Johnson, L. (2015) Advanced Spaceborne

Thermal Emission and Reflection Radiometer Level 1 Precision Terrain Corrected Registered At-Sensor Radiance (AST_L1T) Product, Algorithm Theoretical Basis Document. US Department of the Interior, US Geological Survey. https://doi.org/10.3133/ofr20151171

[63] Cooley, T., Anderson, G.P., Felde, G.W., Hoke, M.L., Ratkowski, A.J., Chetwynd, J.H., *et al*. (2002) FLAASH, a Modtran4-Based Atmospheric Correction Algorithm, Its Application and Validation. *IEEE International Geoscience and Remote Sensing Symposium*, Toronto, 24-28 June 2002, 1414-1418. https://doi.org/10.1109/igarss.2002.1026134

[64] Thome, K., Palluconi, F., Takashima, T. and Masuda, K. (1998) Atmospheric Correction of Aster. *IEEE Transactions on Geoscience and Remote Sensing*, **36**, 1199-1211. https://doi.org/10.1109/36.701026

[65] Abrams, M. (2000) The Advanced Spaceborne Thermal Emission and Reflection Radiometer (ASTER): Data Products for the High Spatial Resolution Imager on Nasa's Terra Platform. *International Journal of Remote Sensing*, **21**, 847-859. https://doi.org/10.1080/014311600210326

[66] Mwaniki, M.W., Moeller, M.S. and Schellmann, G. (2015) A Comparison of Landsat 8 (OLI) and Landsat 7 (ETM+) in Mapping Geology and Visualising Lineaments: A Case Study of Central Region Kenya. *The International Archives of the Photogrammetry, Remote Sensing and Spatial Information Sciences*, **7**, 897-903. https://doi.org/10.5194/isprsarchives-xl-7-w3-897-2015

[67] Marion, A. (1987) Introduction aux techniques de traitement d'image. Editions Eyrolles.

[68] Drury, S.A. (1986) Remote Sensing of Geological Structure in Temperate Agricultural Terrains. *Geological Magazine*, **123**, 113-121. https://doi.org/10.1017/s0016756800029770

[69] Ahmadi, H. and Pekkan, E. (2021) Fault-Based Geological Lineaments Extraction Using Remote Sensing and GIS—A Review. *Geosciences*, **11**, Article 183. https://doi.org/10.3390/geosciences11050183

[70] Irons, J.R., Dwyer, J.L. and Barsi, J.A. (2012) The Next Landsat Satellite: The Landsat Data Continuity Mission. *Remote Sensing of Environment*, **122**, 11-21. https://doi.org/10.1016/j.rse.2011.08.026

[71] Roy, D.P., Wulder, M.A., Loveland, T.R., C.E., W., Allen, R.G., Anderson, M.C., *et al*. (2014) Landsat-8: Science and Product Vision for Terrestrial Global Change Research. *Remote Sensing of Environment*, **145**, 154-172. https://doi.org/10.1016/j.rse.2014.02.001

[72] Huntington, J.F. and Raiche, A.P. (1978) A Multi-Attribute Method for Comparing Geological Lineament Interpretations. *Remote Sensing of Environment*, **7**, 145-161. https://doi.org/10.1016/0034-4257(78)90044-5

[73] Azman, A.I., Talib, J.A. and Sokiman, M.S. (2020) The Integration of Remote Sensing Data for Lineament Mapping in the Semanggol Formation, Northwest Peninsular Malaysia. *IOP Conference Series*: *Earth and Environmental Science*, **540**, Article ID: 012026. https://doi.org/10.1088/1755-1315/540/1/012026

[74] Ramli, M.F., Yusof, N., Yusoff, M.K., Juahir, H. and Shafri, H.Z.M. (2010) Lineament Mapping and Its Application in Landslide Hazard Assessment: A Review. *Bulletin of Engineering Geology and the Environment*, **69**, 215-233. https://doi.org/10.1007/s10064-009-0255-5